applied sciences

MDPI

Review

Dynamic Covalent Bonds in 3D-Printed Polymers: Strategies, Principles, and Applications

Trong Danh Nguyen, My Thi Ngoc Nguyen and Jun Seop Lee *

Department of Materials Science and Engineering, College of Engineering, Gachon University, 1342 Seongnam-daero, Sujeong-gu, Seongnam-si 13120, Gyeonggi-do, Republic of Korea
* Correspondence: junseop@gachon.ac.kr

Abstract

Dynamic covalent bonds within polymer materials have been the subject of ongoing research. These bonds impart polymers, particularly thermosets, with capabilities for self-healing and reprocessing. Concurrently, three-dimensional (3D) printing techniques have undergone rapid advancement and widespread adoption. Since polymers are among the primary materials used in 3D printing, networks featuring dynamic covalent bonds have emerged as a prominent research area. This review outlines approaches for incorporating dynamic covalent bonds into polymers suitable for 3D printing and examines representative studies that leverage these chemistries in material design. Polymers produced using these strategies demonstrate both self-healing and reprocessability, primarily via bond-exchange (metathesis) reactions. In addition, we discuss how the type and amount of dynamic bonds in the network affect the resulting material properties, with particular emphasis on their mechanical, physical, and thermal performance. In particular, the introduction of dynamic covalent bonds seems to significantly improve the degree of anisotropy, which has been the limitation of 3D printing techniques. Finally, we compile recent applications for objects printed from polymers that include dynamic covalent bonds.

Keywords: dynamic covalent bonds; polymer materials; self-healing polymers; 3D printing

check for updates

Received: 15 October 2025
Revised: 28 October 2025
Accepted: 3 November 2025
Published: 4 November 2025

Citation: Nguyen, T.D.; Nguyen, M.T.N.; Lee, J.S. Dynamic Covalent Bonds in 3D-Printed Polymers: Strategies, Principles, and Applications. *Appl. Sci.* **2025**, *15*, 11755. https://doi.org/10.3390/app152111755

Copyright: © 2025 by the authors. Licensee MDPI, Basel, Switzerland. This article is an open access article distributed under the terms and conditions of the Creative Commons Attribution (CC BY) license (https://creativecommons.org/licenses/by/4.0/).

1. Introduction

Three-dimensional (3D) printing is a digital fabrication method first developed in the 1980s [1]. The process constructs objects by adding material layer upon layer, guided by a digital model. Typically, the process begins with the creation of computer-aided design (CAD) files [2]. These models are subsequently translated into layer-by-layer geometries and machine toolpaths using specialized software. This conversion step is essential and must be precisely calibrated based on the selected material, as it can significantly determine the quality of fabricated parts. Major categories of 3D printing technologies include vat photopolymerization, material extrusion, powder bed fusion, binder jetting, material jetting, sheet lamination, and directed energy deposition [3–8]. In comparison to traditional fabrication, 3D printing offers enhanced design versatility but necessitates additional post-processing, stringent process optimization, and often leads to inferior surface finish.

Polymers have emerged as the predominant materials for 3D printing. While specialized formulations have reached commercial markets, continued research is producing new options with enhanced functionalities. Particularly notable is the realization of self-healing and reprocessability through the integration of dynamic covalent chemistry. Several types of reversible bonds, such as disulfide, Diels–Alder, imine, boronate-ester, and hindered

urea, have been systematically investigated for this purpose [9,10]. Beyond imparting adaptability, these dynamic moieties are critical in determining the thermal and mechanical characteristics of 3D-printed networks.

This review examines how dynamic covalent bonds are incorporated into polymer matrices designed for 3D printing (Figure 1). It summarizes literature findings on modifications in material properties resulting from diverse bonding approaches. The review categorizes these outcomes based on the underlying printing mechanisms. In resin-based photocuring techniques, dynamic units are incorporated at the monomer or the oligomer stage. For thermal processing methods, such functionalities are integrated into the polymer filaments themselves. According to recent literature, although various dynamic covalent bonds possess unique properties, they consistently enhance the quality of printed objects. This review highlights these advantages within sections organized by printing methods and bond types. In particular, substantial improvements in uniformity are observed, as reflected by reductions in the resulting degree of anisotropy (D_a). The review concludes by briefly considering recent applications of these adaptive materials in the field of additive manufacturing.

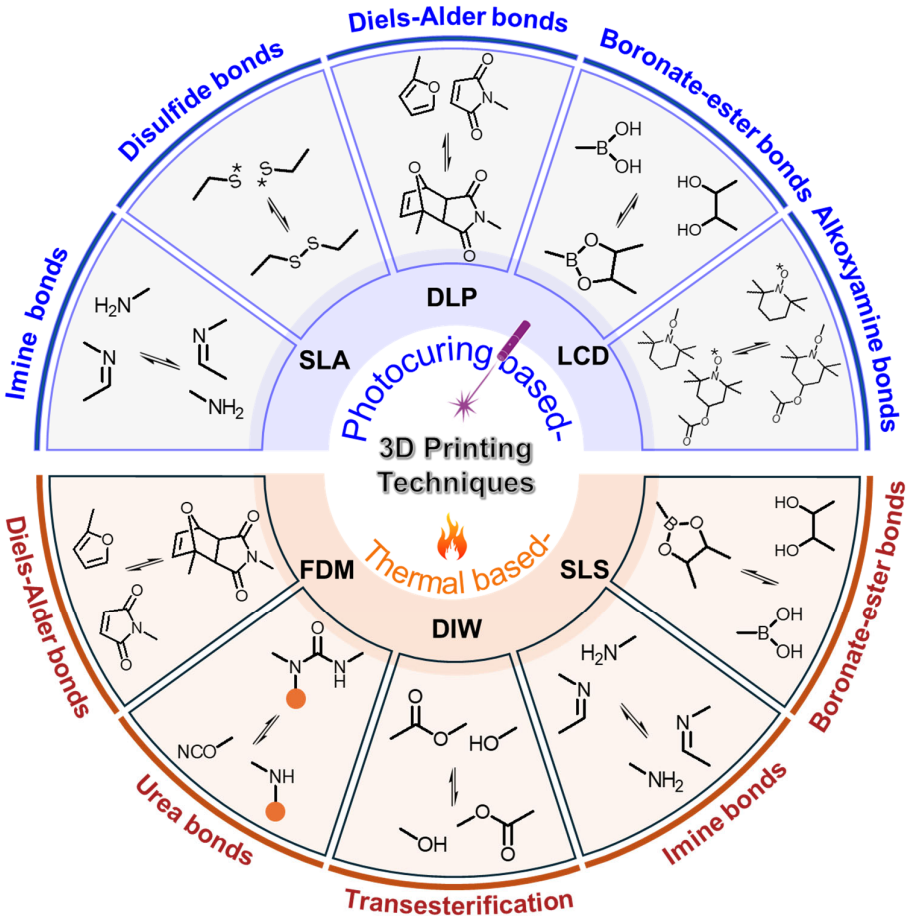


Figure 1. Dynamic covalent bonds in the polymer materials used in three-dimensional printing techniques.

2. Mechanism of 3D Printing Technique

2.1. Three-Dimensional Printing Technique Based on Light Irradiation

Vat photopolymerization (VPP)-based 3D printing utilizes photo-curable resins as the main raw materials. In typical polymer studies, these resins are composed of monomers (or oligomers), crosslinkers, photoinitiators, and, in some cases, solvents. Photopolymerization, initiated by photoinitiators upon exposure to light, leads to the formation of polymeric

networks. The required activation wavelength may range from ultraviolet (UV-C) to near-infrared (NIR), depending on the photoinitiator implemented [11–13]. Solvents not only ensure uniform distribution of resin ingredients but also assist in polymerization efficiency and viscosity adjustment. Due to its reliance on monomer polymerization, the VPP approach offers several intrinsic benefits.

Firstly, photopolymerization allows for selective curing, which is crucial for constructing intricate geometries. The literature reports resolutions ranging from the nanometer scale to several micrometers [14,15]. The printing speed can be adjusted by manipulating the reaction kinetics, which depend on parameters such as monomer structure and light intensity [16]. Moreover, incorporating photoabsorbers enhances process accuracy by controlling cure depth (Z-resolution), reducing scattering, and suppressing unintended polymerization beyond the target area [17,18]. Robust interlayer adhesion is achieved because each successive layer undergoes polymerization directly at the interface with the preceding layer, resulting in isotropic mechanical performance, a challenge often present in thermal-based approaches. Additionally, the relatively mild thermal stress encountered during curing promotes dimensional stability and preserves material properties compared with heat-driven methodologies.

Despite these strengths, VPP contends with ongoing challenges. Post-processing is necessary to eliminate residual or trapped resin, generally using solvent washing. Selection of an inappropriate solvent can lead to swelling of the printed structure, and therefore solvent choice requires careful optimization. Supplemental post-curing procedures, such as UV or thermal exposure, may be necessary based on specific resin chemistries. VPP materials ultimately form thermoset crosslinked polymer networks that exhibit superior mechanical properties but fundamentally limit recyclability. Currently, there are three primary types of VPP: stereolithography (SLA), liquid crystal display (LCD), and digital light processing (DLP) (Figure 2). Research in VPP printing continues to expand across multiple fields of applications [19–23]. Meanwhile, a variety of new materials have also been utilized in this printing technique besides polymer resins, such as hydrogels and ceramics materials [24–27].

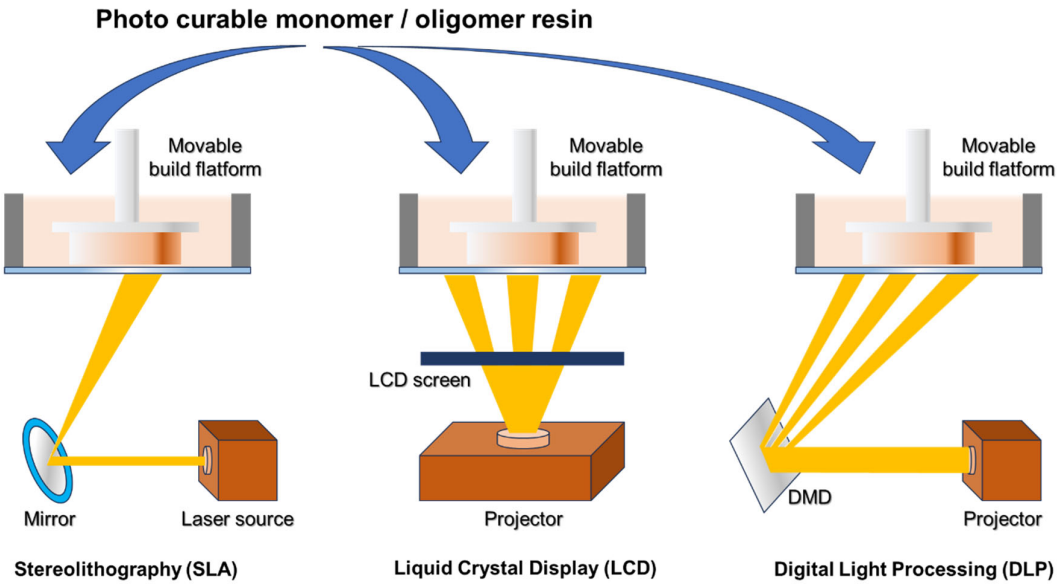


Figure 2. The varieties of vat photopolymerization (VPP) 3D printing techniques used for materials containing dynamic covalent bonds, including stereolithography (SLA), digital light processing (DLP), and liquid crystal display (LCD).

2.1.1. Stereolithography (SLA)

The first generation of stereolithography (SLA) emerged in 1984, and the technique has since evolved due to inherent advantages that alternative systems have not been able to surpass [28]. SLA functions by directing a coherent UV laser to initiate polymerization at the voxel level. This approach provides meticulous control over light exposure, resulting in superior resolution, capability to produce larger structures, and facilitating top-down printing processes. A top-down setup negates the need to detach cured layers from the bottom window, circumventing a significant issue present in bottom-up configurations. Nevertheless, top-down arrangements introduce challenges, such as requiring an extensive resin reservoir to accommodate the build volume and ensuring a consistently stable resin surface as fabrication progresses. While SLA is typically slower in comparison to techniques that cure full layers at once, its resolution is often regarded as a more critical advantage. Significantly, the development of two-photon polymerization (also known as direct laser writing, DLW) has enabled resolutions below 100 nm and surface roughness under 10 nm [29,30]. In contrast to traditional SLA, this method utilizes photoinitiators responsive to highly focused near-infrared (NIR) irradiation [31]. The higher wavelength helps overcome the diffraction barrier and supports the creation of intricate architectures, expanding its utility in advanced applications including microrobotics [32].

2.1.2. Liquid Crystal Display (LCD)

Unlike SLA, liquid crystal display (LCD)-based printing utilizes a projector to emit UV light, which initiates photopolymerization in a layer-by-layer manner. The configuration of each layer is determined by channeling the light through the LCD screen, which functions as a dynamic mask. Bertsch et al. first reported this method in 1997 [33]. Due to restricted resolution at that time, digital light processing (DLP) technology was introduced as an alternative approach. Despite these initial challenges, LCD technology has steadily progressed, primarily propelled by innovations in display technologies. Although LCD systems are generally more cost-effective, a significant limitation is the reduced durability of the panels when subjected to continuous UV illumination, particularly at wavelengths below 400 nm, which poses significant concerns for extended usage [34]. To mitigate this, various photoinitiators have been developed for activation with wavelengths above 400 nm, and projectors are now capable of using LEDs at 405 nm [35]. Therefore, LCD-based printing continues to present a practical and cost-effective method with considerable scope for future advancements and broader application.

2.1.3. Digital Light Processing (DLP)

Digital light processing (DLP) is a layer-by-layer additive manufacturing technique, first introduced in 1998 when Laurence et al. enhanced printing resolution by replacing the LCD screen with a digital micromirror device (DMD) [36,37]. In DLP, a projector illuminates UV light through engineered patterns to initiate photopolymerization [38,39]. The DMD, composed of an orthogonal array of individually addressable aluminum micromirrors, serves as the essential component in DLP [40]. By selectively directing and reflecting light onto the resin bath, the system facilitates rapid solidification of whole layers, leading to increased printing speed. The functionality of the DMD depends on the swift rotation of its micromirrors, typically operating at kHz frequencies. Despite the limited range of rotation angles, the system maintains higher stability compared with conventional projectors or LCD panels, representing a significant benefit for DLP printing. Nevertheless, DLP technology has intrinsic constraints as follows: the fixed dimensions of both the projector and DMD limit the attainable resolution and the maximum printable area in the X–Y plane. In most

practical implementations, DLP is arranged in a bottom-up orientation, enabling precise focusing of light on the resin surface during fabrication.

2.2. Three-Dimensional Printing Technique Based on the Temperature

Besides VPP-based 3D printing, thermal processing techniques are also extensively utilized. In this context, thermal processing encompasses methods in which the printing material is softened, melted, or sintered through the application of heat [41,42]. By heating the material above a transition temperature, depositing it sequentially in layers, and subsequently allowing it to solidify, strong interlayer adhesion can be established. This mechanism enables temperature-responsive materials such as thermoplastics, ceramics, metals, and their composites to be manufactured into intricate 3D architectures [43,44]. In contrast, conventional thermosets are incompatible with this method, as their exceedingly long stress relaxation times impede adequate interdiffusion of molecular chains [45–48]. As a result, this limitation narrows the portfolio of printable materials and precludes the exploitation of the notable properties of thermoset polymers, including superior mechanical performance, outstanding thermal stability, and robust chemical resistance [49]. Addressing this issue requires dynamic covalent bonds in advanced thermoset systems to provide rapid exchange kinetics during the printing process, ensuring robust cohesion at powder particle or interlayer interfaces, while also maintaining sufficient chemical stability to enable recyclability, welding, and related applications [50,51]. Consequently, it is essential to have a comprehensive understanding of the working principles underlying each thermal technique, the appropriateness of specific dynamic covalent bonds, and their functional roles during fabrication. In this section, three representative thermal 3D printing methods, fused deposition modeling (FDM), direct ink writing (DIW), and selective laser sintering (SLS), are introduced and examined in depth in the subsequent sections (Figure 3). The research of thermal-based printing also has numerous achievements in new techniques and materials [52–54].

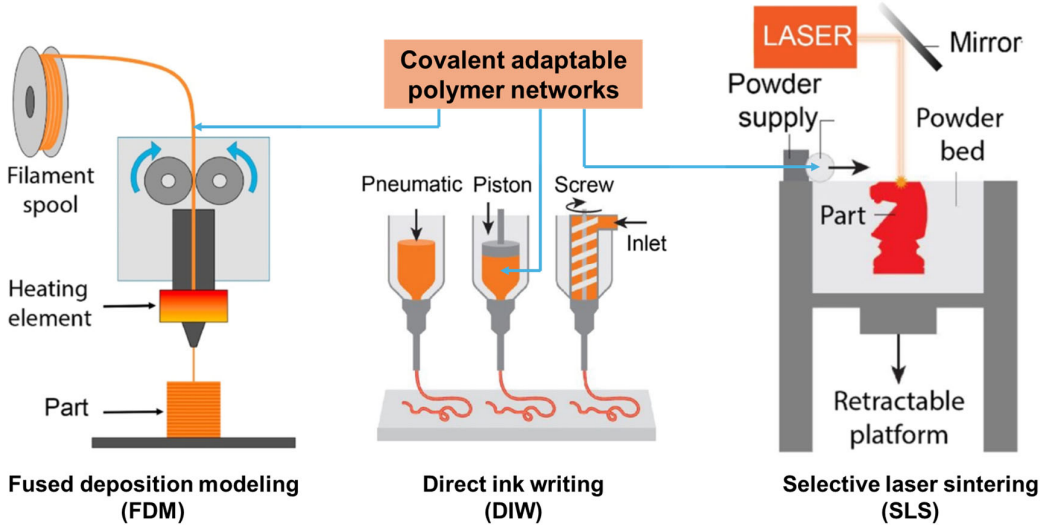


Figure 3. Three representative thermal 3D printing techniques, fused deposition modeling (FDM), direct ink writing (DIW), and selective laser sintering (SLS) [55]. Copyright 2024, IOP Science.

2.2.1. Fused Deposition Modeling (FDM)

In 1988, the fused deposition modeling (FDM) technique—also referred to as fused filament fabrication (FFF)—was introduced by S. Scott Crump for the fabrication of thermoplastic-based 3D structures [56]. In this process, a thermoplastic filament of uniform diameter is drawn from a spool into a heated nozzle enclosed within a motion-controlled system, which extrudes and deposits the molten polymer onto designated areas of the

build platform. At the start of printing, the platform is positioned near the nozzle tip, while a stepper-motor-driven gear advances the filament into the hot end, where it softens or melts. The liquefied thermoplastic is extruded layer-by-layer, with the platform descending after each layer by a set thickness until the 3D object is completed. Beyond conventional filament-based feedstocks, recent advances have enabled filament-free systems that directly process thermoplastic pellets or powders.

Although FDM is a relatively user-friendly and cost-efficient method, achieving optimal mechanical performance requires precise control of numerous parameters, broadly classified as manufacturing and structural. Among manufacturing parameters are factors such as extrusion temperature, printing speed (or deposition rate), build platform temperature, and ambient temperature [57]. For instance, increasing print speed can enhance manufacturing efficiency but may also reduce filament fusion and result in weak interlayer bonding, while excessively slow speeds might lead to filament swelling, poor deposition quality, and difficulties in layer bonding [58]. Additionally, extrusion temperature profoundly impacts polymer crystallinity, thus influencing both the strength and toughness of the printed structure [59]. Structural parameters (such as raster spacing, layer gaps, and part orientation) govern interfacial adhesion quality and anisotropy in the final product. Systematic optimization of these factors enables the production of FDM components with improved structural reliability and functional performance.

2.2.2. Direct Ink Writing (DIW)

Direct ink writing (DIW) was first introduced by Cesarano and Calvert in a 1997 patent filed at Sandia National Laboratories [60]. While DIW and FDM both operate based on material extrusion, DIW utilizes a pressure-controlled syringe extruder to dispense viscoelastic inks instead of solid filaments. In certain implementations, the extruder is integrated with a heating component—for instance, when dynamic covalent bond-containing polymers serve as inks, supplementary heat may be necessary to initiate associative or dissociative exchange reactions during the printing process [61–63]. Unlike FDM, DIW fundamentally relies on the rheological characteristics of the ink to ensure the printed form remains stable after extrusion [64]. The inks are formulated to possess high viscosity (103–106 mPa·s) and to demonstrate shear-thinning (pseudoplastic) behavior, which not only enables smooth extrusion through the nozzle but also ensures the deposited structures retain their shape [65]. Aside from its specific material requirements, DIW uses a layer-by-layer deposition sequence analogous to that of the FDM technique. Frequently, objects fabricated via DIW undergo oven curing or equivalent post-processing methods, as gel-like materials generally require prolonged periods to achieve complete solidification at ambient conditions.

Similar to other extrusion-based technologies, critical parameters such as nozzle diameter, applied extrusion pressure, and print speed largely determine printing precision and fidelity. Reducing nozzle diameter enhances resolution of printed features, but this typically necessitates higher extrusion pressures and extends fabrication times, which increases the likelihood of nozzle blockage. Moreover, slower printing speed can yield improved dimensional accuracy and achieve smoother surfaces, although this results in lower production throughput. DIW is established as a relatively straightforward, adaptable, and economically advantageous approach that accommodates diverse material systems, including ceramics, metals, polymers, composites, and notably viscoelastic inks for soft and biological applications. Consequently, DIW has found broad utility in bio-printing (e.g., tissue scaffolds), soft robotics, energy storage devices such as batteries and supercapacitors, electronics, and the fabrication of lightweight metamaterial lattice structures [66].

2.2.3. Selective Laser Sintering (SLS)

Selective laser sintering (SLS) was initially introduced by Deckard in 1986 at the University of Texas [67]. Unlike extrusion-based techniques, SLS utilizes a high-power laser as the heat source to selectively fuse powder particles on the powder bed surface [68]. During operation, a roller spreads a uniform layer of powder onto the build platform. The laser then scans and selectively sinters the areas corresponding to the object's cross-section, causing the illuminated powder particles to coalesce into a coherent layer. After sintering, the build platform descends by one layer thickness, and a fresh layer of powder is applied. This cycle continues until the entire 3D object is fabricated [69].

One of the main benefits of SLS, compared to extrusion- and vat-photopolymerization-based techniques, is that it eliminates the need for support structures: the unsintered powder acts as a natural support for the part throughout fabrication [70]. This characteristic allows for the fabrication of intricate geometries, such as internal channels and lattice frameworks. Despite these advantages, SLS presents notable limitations, including challenges with powder handling and reuse, precise thermal regulation, increased surface roughness, dimensional inaccuracy, significant equipment expense, and the requirement for extensive post-processing [71]. As an example, repeated exposure of powders to heat during processing can deteriorate their properties, resulting in reduced mechanical strength and compromised surface integrity [72,73]. Additionally, elevated sintering temperatures may lead to warping and shrinkage in polymer-based specimens.

The ultimate characteristics of SLS-printed objects are determined by both material properties (e.g., powder particle size distribution, shape, and flowability) and laser-processing parameters (e.g., laser power, scan speed, layer thickness, hatch spacing, and energy distribution). For example, porosity is one of the primary challenges encountered in SLS. Porosity can arise due to trapped air between powder particles, improper scan speeds or laser powers, or misaligned layers, resulting in interlayer voids [74,75]. Consequently, careful optimization and a comprehensive understanding of these parameters are needed to produce dense, mechanically robust parts. When SLS powders comprise polymers with dynamic covalent bonds, the kinetics of bond-exchange are of particular significance. The dynamic covalent bonds must undergo rapid exchange during sintering to promote effective particle–particle fusion, thus guaranteeing strong interlayer adhesion and desirable mechanical integrity in the produced object.

3. Reversible Dynamic Covalent Bonding in 3D Printing

Incorporating dynamic covalent bonds within materials can impart reprocessability and self-healing capabilities, which is particularly advantageous as printed objects are prone to damage before any post-processing steps. The presence of these bonds also contributes to reducing polymer waste and improving the environmental sustainability of polymer materials [76]. Furthermore, dynamic covalent bonds can alter the morphology of polymer networks, thereby influencing the overall material properties [77–79]. Properties that may be affected include physical and thermal characteristics, as well as polymer conductivity [80].

3.1. Mechanism of Dynamic Covalent Bonds and Their Influence in 3D Printing

The dynamic covalent bonds have the ability to allow metathesis reaction, also known as exchange reactions. As the name implies, these reactions allow dynamic bonds to exchange the polymers carrying them. Whether through associative or dissociative mechanisms, dynamic covalent bonds bestow both self-healing and reprocessing abilities to materials.

However, just self-healing and reprocessing are not enough for these networks to attract such strong attention. In 3D printing, the mechanism of printing layer-by-layer leads to weak interfaces, which becomes the weakest points in the object's mechanical properties. Such weakness is displayed as the degree of anisotropy (D_a), demonstrated through differences between results of different angles tensile tests. Both strength and elongation are used for comparison. Specimens printed at 0° and 90° raster angles are most commonly used to investigate D_a [81]; however, other angles such as 30°, 45°, and 60° can also be used for different study purposes [82]. On the other hand, D_a affects not only mechanical properties but also extends its influence toward electrical and thermal properties, thereby becoming one of the biggest challenges that needs to be overcome [83–85]. The metathesis reactions of the dynamic covalent bonds can address such limitations by creating new strong interlayer connections through post-printing treatment process as displayed in Figure 4. Though the efficiencies are to be discussed, multiples recent publications proposed in the following sections still show the potential of dynamic covalent bonds in 3D printing.

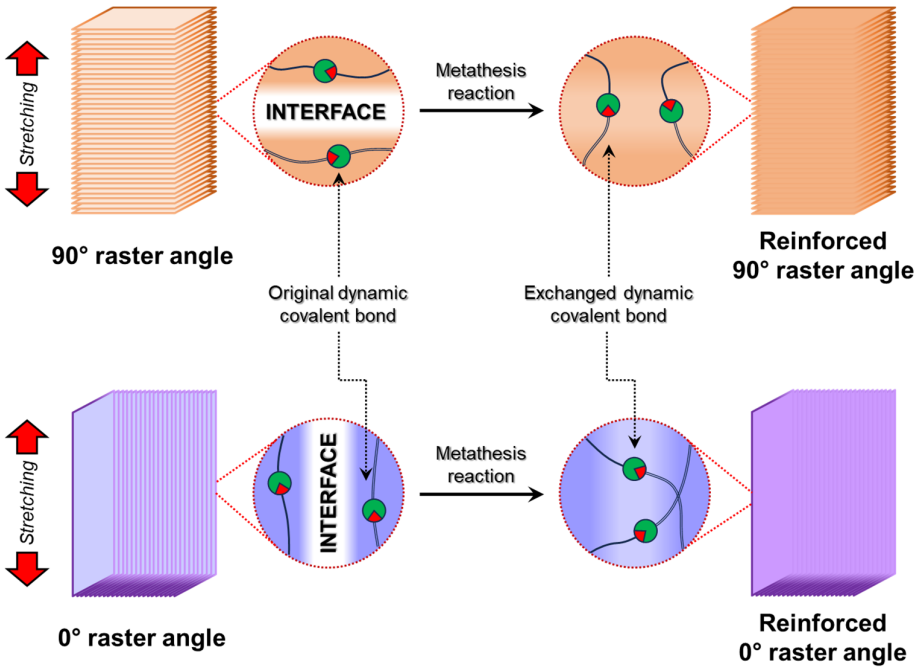


Figure 4. The interlayer connections formed through metathesis reaction of dynamic covalent bonds.

3.2. The Introduction of Dynamic Covalent Bonds in Light-Based 3D Printing

3.2.1. Imine Covalent Bonds

Imine dynamic covalent bonds represent a class of bonds that can undergo metathesis in response to appropriate stimuli. These bonds form through a condensation reaction between aldehydes or ketones and primary amines. Metathesis facilitates not only self-healing but also enhances weldability and stress relaxation in 3D-printing applications [86]. Enhanced weldability allows printed polymer segments to fuse together, while stress relaxation ensures that internal stress from curing is dissipated within the network. As a result, imine-functionalized polymer networks have strong potential for fabricating structurally stable printed objects.

A study by Vilanova-Pérez et al. demonstrated the incorporation of imine bonds into a polymer network fabricated via DLP (Figure 5a) [87]. While vanillin methacrylate was synthesized from vanillin using 4-(dimethylamino)pyridine, the research also explored interactions between various photoinitiators and the imine functionality. The authors proposed that photoinitiators might facilitate metathesis given the parallels observed in thermally and UV-cured systems. The experimental results showed that phosphine oxide

initiators, such as diphenyl(2,4,6-trimethylbenzoyl)phosphine oxide (TPO) and bis(2,4,6-trimethylbenzoyl)phenylphosphine oxide (BAPO), act as catalysts in the metathesis reaction. In addition, the hydrolysis behavior of imine bonds in a range of solvents was systematically evaluated. Notably, carbon-backbone hydrophilicity strongly influenced imine hydrolysis regardless of the presence of hydrochloric acid, a well-known promoter of imine dissociation. These results highlight that the tunable reversibility of imine-based polymers may facilitate expanded applications.

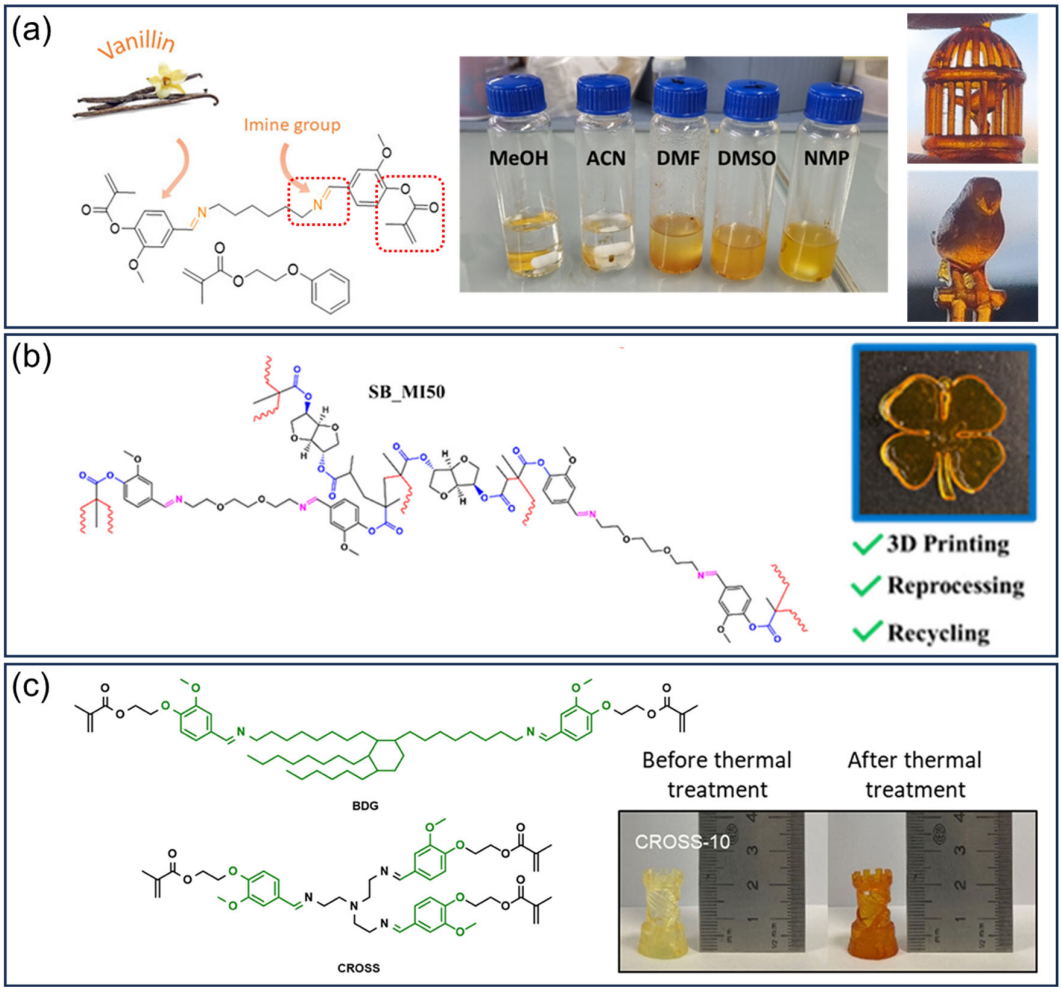


Figure 5. (**a**) 3D-printed network contains imine dynamic covalent bonds printed based on a monomer synthesized from Vanillin [87]. Copyright 2024, American Chemical Society. (**b**) The reprocessable and recyclable polymer network containing imine bonds for the application of VPP printing [88]. Copyright 2023, American Chemical Society. (**c**) The thermally stable polymer for 3D printing that has reprocessability thanks to the imine bonds present in the network [89]. Copyright 2023, American Chemical Society.

Linear polymer networks are capable of melting and being reshaped, in contrast to 3D covalently crosslinked networks that maintain their shape upon heating since their chains are permanently bonded and are not reprocessable. Introducing dynamic covalent bonds as crosslinkers enables reprocessing through reversible metathesis. Liguori et al. investigated the reprocessing of printed materials by systematically varying monomer ratios (Figure 5b) [88]. Methacrylated isosorbide provided enhanced rigidity to address common solubility issues associated with biobased diluents, while a spacer monomer based on methacrylated vanillin facilitated uniform and consistent curing of the material. The final polymer could be readily reprocessed and efficiently degraded under basic conditions.

Thus, the influence of monomer structure was clearly stated alongside the introduction of dynamic covalent bonds.

Stouten et al. described imine-functionalized printed materials and systematically compared their shape retention to commercial acrylonitrile–butadiene–styrene (ABS) and polylactic acid (PLA) (Figure 5c) [89]. The ability of imine bonds to undergo metathesis inhibits chain mobility at temperatures exceeding the material's melting point, thereby allowing printed structures to maintain their shape. In contrast, the imposition of mechanical force was found to induce metathesis among distant imine bonds, enabling the network to be reprocessed. The investigation also included a systematic study of imine crosslink concentration, establishing that the density of crosslinks plays a pivotal role in determining both reprocessability and network properties.

3.2.2. Disulfide

Disulfide exchange is a well-established dynamic covalent motif that is commonly incorporated into polymer networks. This bond is formed through the oxidation of two thiol groups, with typical oxidants including H_2O_2/NaI, $NaIO_4$, KIO_4, and iodobenzene diacetate [90–93]. The necessity of post-washing to remove residual oxidants poses a practical challenge that has limited broader application. Nevertheless, these reactions offer substantial operational simplicity, which is a significant advantage. Beyond having a bond energy similar to that of C–C linkages in polymer backbones, disulfide exchange is amenable to activation by heat or UV irradiation [94,95]. Thus, UV irradiation can act as a post-treatment strategy for 3D-printed constructs, as illustrated in the work of Wang et al. (Figure 6a) [96]. Not only were the printed layers efficiently bonded, but the dynamic metathesis reaction also enhanced stress relaxation and improved material properties [97]. By adjusting the disulfide content, the impact of disulfide-containing monomers on polymer characteristics was systematically revealed. The researchers further reported shape recovery and reprogrammability as a result of bond-exchange processes. Employing a distinct strategy, Olikagu et al. addressed the challenge of monomer cost, which limits vat photopolymerization, by utilizing economical elemental sulfur for the synthesis of sulfur monochloride (S_2Cl_2), a precursor to the disulfide methacrylate monomer (Figure 6b) [98]. The resulting polymer possessed high transparency, supporting optical lens preparation by VPP, and was confirmed to be non-toxic and compatible with cell culture.

In contrast to the aforementioned studies, Li et al. synthesized an acrylate-terminated urethane oligomer incorporating disulfide bonds, combined with hydroxyethyl acrylate (HEA) and a photoinitiator, and employed the mixture as a resin for VPP 3D printing (Figure 6c) [99]. The prepared materials inherited the superior stretchability of the oligomer, achieving nearly 400% strain. The presence of disulfide exchange endowed the network with self-healing properties, promoted by high chain mobility. While oligomers can cause an increase in resin viscosity, the incorporation of HEA as a reactive diluent enabled poly(hydroxyethyl acrylate) formation, which linked the polymer network and, according to the authors, supported rapid printing.

3.2.3. Diel–Alders

Diels–Alder (DA) linkages are a type of dynamic covalent bond created between a dienophile and a diene through a [4+2] cycloaddition reaction [100]. Like other dynamic covalent chemistries, DA units are incorporated into polymer networks at either the monomer or oligomer stage. Unlike many comparable reactions, the cycloaddition proceeds rapidly without the requirement for acids/bases, metals, or radicals. Additionally, the thermal reversibility of DA adducts facilitates self-healing and reprocessability [101,102].

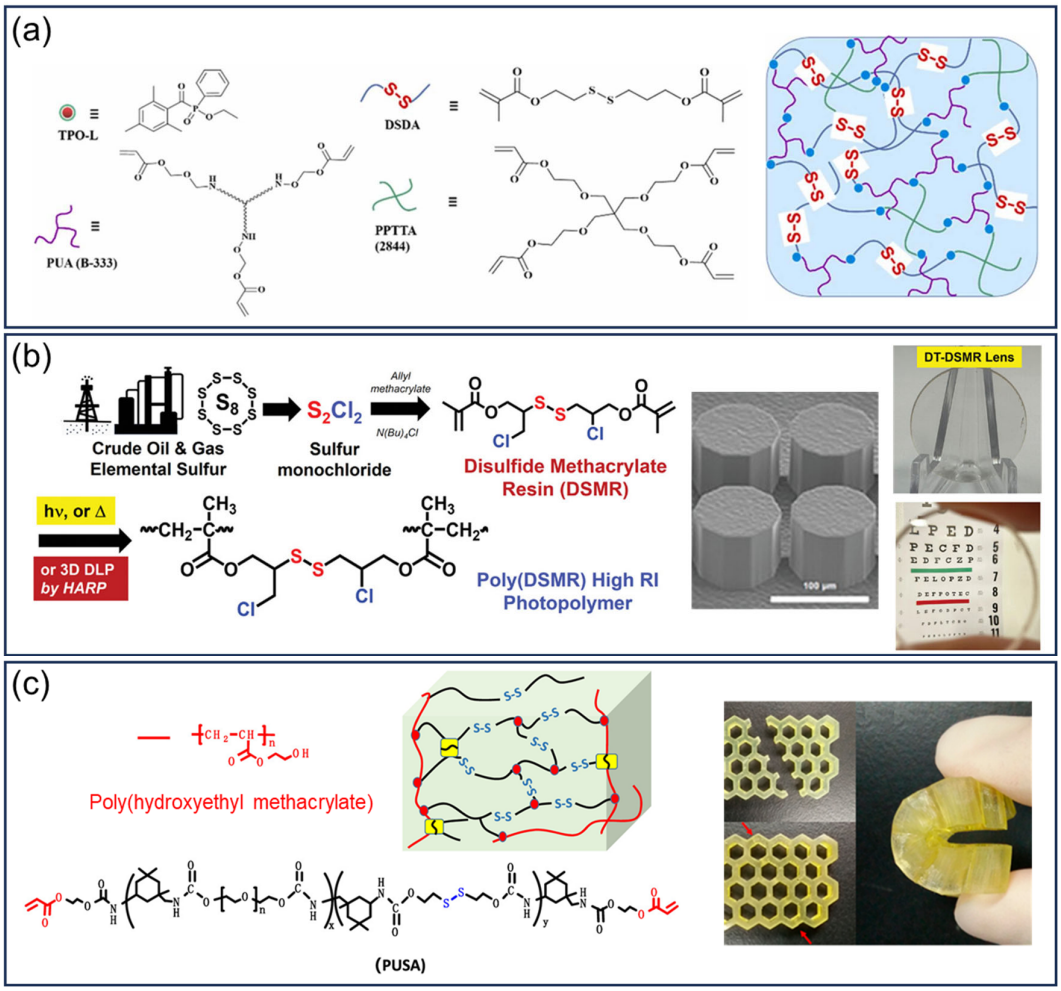


Figure 6. (**a**) Introduction of monomer containing disulfide into polymer network for stress relaxation [96]. Copyright 2022, Elsevier. (**b**) Low-cost production of disulfide-containing monomer for the application of lens production (the red arrows indicate the healed line of cut samples) [98]. Copyright 2025, John Wiley and Sons. (**c**) The network built from disulfide bonds contained oligomer and hydroxyethyl acrylate monomer for VPP 3D printing [99]. Copyright 2019, American Chemical Society.

Despite these benefits, excessive DA adducts can result in reduced shape retention. The inherent flow associated with the retro-DA reaction can lead to deformation and rough surface texture in printed objects [103]. A work by Durand-Silva et al. demonstrate that both shape stability and healing efficiency are influenced by DA content (Figure 7a) [104]. An excessive concentration of DA units promotes loss of structural integrity, whereas insufficient DA content decreases self-healing performance. Their findings further revealed that the mechanical properties vary with DA concentration. In a related study, Li et al. established three networks possessing distinct DA contents by introducing DA functionality via a urethane-based oligomer (Figure 7b) [105]. The DA component was introduced in the material through an oligomer structured from urethane bonds. Similar to the findings above, increasing the DA-oligomer proportion enhanced the hardness of the samples while improving self-healing behavior. Dynamic mechanical analysis revealed that a higher DA content elevated the glass-transition temperature (T_g), which in turn influenced the material's capacity for reprocessing.

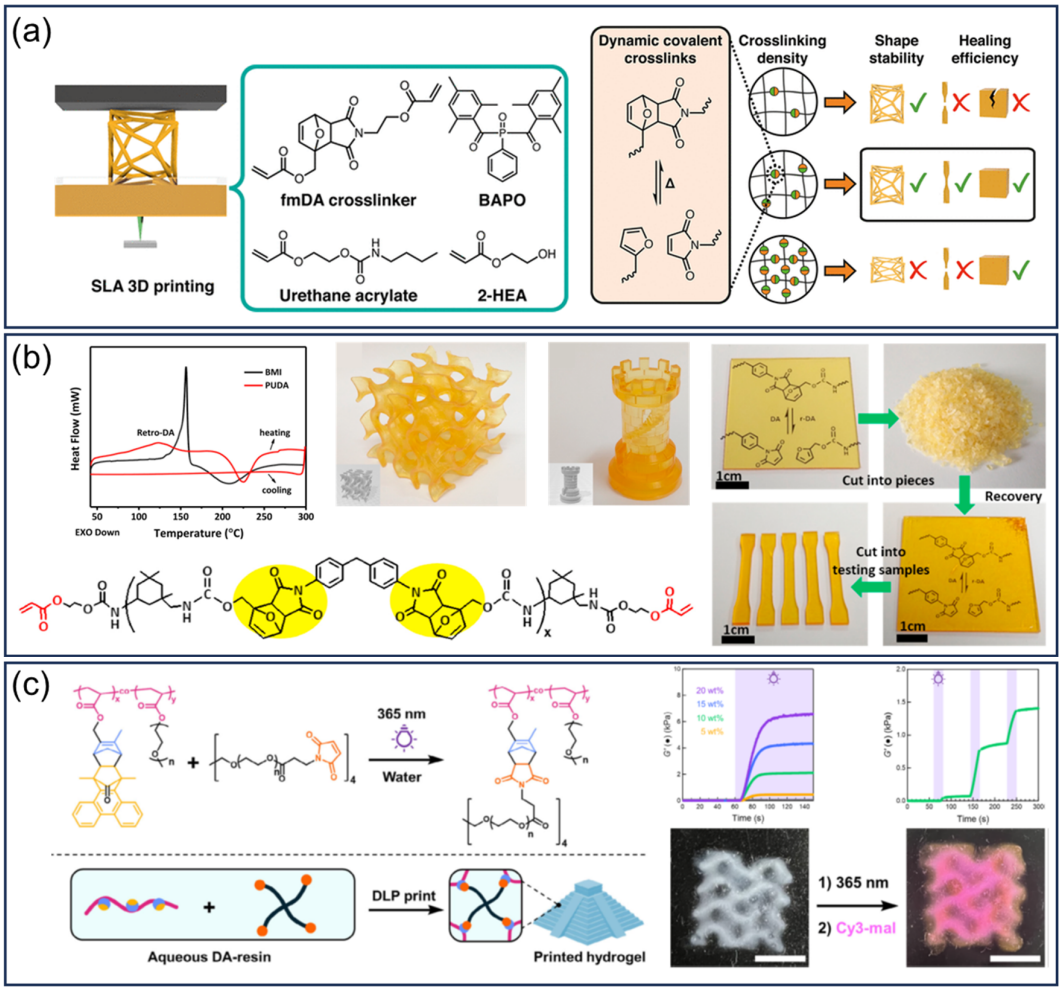


Figure 7. (**a**) Effect of Diels–Alder (DA) concentrations on the shape stability and self-healing efficiency of the polymer material [104]. Copyright 2021, American Chemical Society. (**b**) The effect of DA on thermal properties of the polymers and their reprocessability [105]. Copyright 2020, Elsevier. (**c**) The printing strategy utilizing the dissociation of cyclopentadienone–norbornadiene DA adduct under of 365 nm UV irradiation [106]. Copyright 2025, John Wiley and Sons.

Conversely, Kaneko et al. harnessed DA chemistry to produce VPP-printed 3D networks in the absence of photoinitiators (Figure 7c) [106]. In this strategy, preinstalled cyclopentadienone–norbornadiene (CPD–NBD) DA adducts dissociate under exposure to 365 nm irradiation, releasing reactive cyclopentadiene for subsequent DA bond formation. As a consequence, printing without radical initiation became feasible, and the materials were further functionalized with cyanine3-maleimide and cyanine5-maleimide. While high curing rates were observed, the entire printing process may still be limited in speed by the series of reaction steps required in comparison to traditional photopolymerization of multifunctional methacrylates.

3.2.4. Boronate Ester

Boronate ester represents another type of dynamic covalent bond incorporated into polymer networks for VPP 3D printing. These bonds are formed between boronic acids and diols. While the formation of boronate esters is relatively simple, the equilibrium is highly sensitive to water and, to a lesser degree, to pH and the geometry of the diol (e.g., cis-1,2- or 1,3-diols) [107]. Therefore, drying agents such as Na_2SO_4 and $MgSO_4$ are used to eliminate both residual moisture and water generated during esterification [108,109]. This sensitivity to moisture and temperature allows for facile exchange reactions within the material [110].

Based on this principle, Bonacini et al. developed a post-treatment process in which, in addition to UV irradiation, printed components were heated to 80 °C to promote exchange reactions and transform the as-printed layered structure into a more homogeneous network (Figure 8a) [111]. The inclusion of boronate–ester linkages and their exchange dynamics reduced the degree of anisotropy (D_a), which assessed the physical properties of samples printed at both 0° and 90° orientations. Moreover, the post-curing heating process aided in relaxing internal stress within the material.

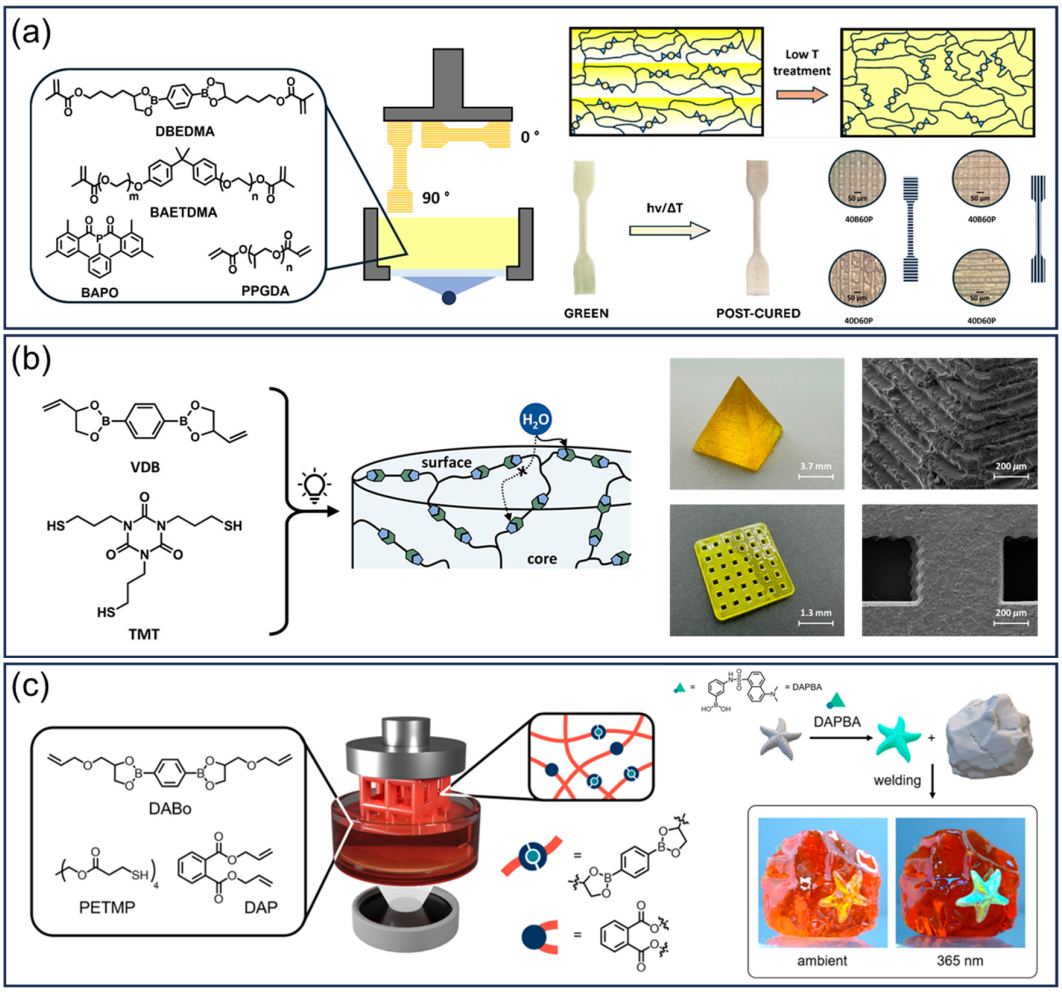


Figure 8. (**a**) The metathesis reaction of boronate–ester bond during the post-treatment of a 3D-printed object to achieve a homogeneous network [111]. Copyright 2025, American Chemical Society. (**b**) Degradable 3D-printed polymer networks generated by monomers carry boronate–ester dynamic covalent bond [112]. Copyright 2023, American Chemical Society. (**c**) Printable, degradable, and modifiable polymer network developed based on monomers containing boronate–ester bonds [113]. Copyright 2021, American Chemical Society.

In a different approach, boronate ester dynamics enabled Sinawehl et al. to develop a printable, degradable polymer with high conversion and low levels of unreacted monomer (Figure 8b) [112]. The dynamic bonds allowed for controllable degradation, especially under aqueous or basic conditions, which supports applications in biomedicine, scaffold fabrication, and environmentally sustainable materials. Similarly focusing on degradable systems, Robinson et al. synthesized a polymer network with boronate–ester bonds and further demonstrated the ability to weld distinct parts through bond-exchange (Figure 8c) [113]. They also achieved molecular-level modification by functionalizing the surface with 3-(dansylamino)phenylboronic acid, thereby creating a hybrid system with both fluorescent

and non-fluorescent domains. Collectively, these investigations demonstrate that careful selection of boronic acid/diol combinations, regulation of process temperature, and appropriate post-treatment strategies can optimize print quality, interlayer adhesion, potential for recycling, and tailored degradation in VPP-fabricated polymers.

3.2.5. Alkoxyamine

Alkoxyamine linkages are a type of dynamic covalent bond that can reversibly homolyze to yield a persistent nitroxide radical and a transient carbon-centered radical. Beyond facilitating the nitroxide exchange reaction (NER), the persistent nitroxide may also function as a mediator for nitroxide-mediated polymerization (NMP) [114]. In contrast to NER, NMP leads to irreversible chain extension. The properties of alkoxyamines, including their stability and reactivity, are tunable through the design of the nitroxide structure (involving modifications to steric bulk, electronic properties, and substituents) [115,116]. Numerous adaptable polymer networks have been created via NMP initiated from alkoxyamine-functional motifs. Nonetheless, potential side reactions, such as radical-induced processes and irreversible bond cleavage, must be carefully considered during the design and development of materials [117].

The distinct functions of NER and NMP are exemplified in the adaptive network developed by Tran et al. (Figure 9a) [118]. In this system, NMP promoted network growth by polymerizing polystyrene chains, whereas NER induced de-growth by breaking crosslinks containing alkoxyamine units when free TEMPO (2,2,6,6-tetramethylpiperidine-1-oxyl) was present. This multi-modal adaptability enabled printed structures to undergo changes in size, color, and mechanical properties. Building on this strategy, Jia et al. designed an adaptable polymer network that exploits the interplay of NER and NMP (Figure 9b) [119]. Their study also examined the impact of both NER and NMP on the swelling and thermal response of the printed polymer network.

Taking an alternative approach, Wu et al. investigated the surface modification of alkoxyamine-containing networks (Figure 9c) [120]. Utilizing a specifically designed nitrone structure, the authors converted the thermal C–ON dissociation process into a photochemical one, thus facilitating nitroxide-mediated photopolymerization (NMP2) [121,122]. Within this framework, photopolymerization of the monomer leads to the formation of alkoxyamine directly within the network during VPP 3D printing, thereby incorporating dynamic linkages into the polymer backbone. As a result, it becomes possible to modify the geometry of printed objects at both micro- and macro-scales by employing NMP2 through laser irradiation at appropriate wavelengths and intensities.

3.3. The Introduction of Dynamic Covalent Bonds in Thermal 3D Printing

3.3.1. Diel–Alders

The DA metathesis reaction, in which dissociation (the retro reaction) occurs at a higher temperature than the reformation reaction, appears well-suited for thermal-based 3D printing. During commercial polymer extrusion, the feed melts at the nozzle as it is deposited. The molten state is characterized by high viscosity. While this viscosity maintains shape fidelity throughout the printing process, it also limits interlayer chain diffusion and bonding, thereby exacerbating anisotropy (D_a) [123].

This limitation can be addressed by employing the metathesis reaction of dynamic bonding, specifically the DA reaction, as described in the report by Bischoff et al. and depicted in Figure 10a [124]. Thermal dissociation of DA linkages temporarily disrupts the network into lower-viscosity species, such as monomers or oligomers. These mobile entities from adjacent layers can reestablish DA bonds across interfaces, effectively reducing D_a. However, exceeding an optimal DA content leads to the disadvantages discussed previously.

To mitigate this, the authors added polycaprolactone as a secondary phase to enhance mechanical strength. Another important factor is the kinetics of DA reformation. The authors reported recrystallization occurring within approximately 10 min, which promotes improved interlayer adhesion, although it raises potential concerns regarding overall printing throughput. In contrast, the DA retro reaction presented a more effective method for fabricating composite materials, as demonstrated by Ouyang et al. (Figure 10b) [125]. The metathesis reaction not only lowers the D_a but also enabled enhanced infiltration of polymers into the carbon nanotube (CNT) filler during SLS printing. While the DA-based polymer particles were simply coated with CNTs using liquid deposition, the resulting composite block demonstrated uniform CNT filler distribution. Zhou et al. focused on another aspect by investigating property changes resulting from varying concentrations of the bismaleimide crosslinker, which in turn altered the DA concentration (Figure 10c) [126]. The authors concluded that not only can the material's properties be tuned, but the presence of DA also facilitated efficient connection of blocks with differing designs.

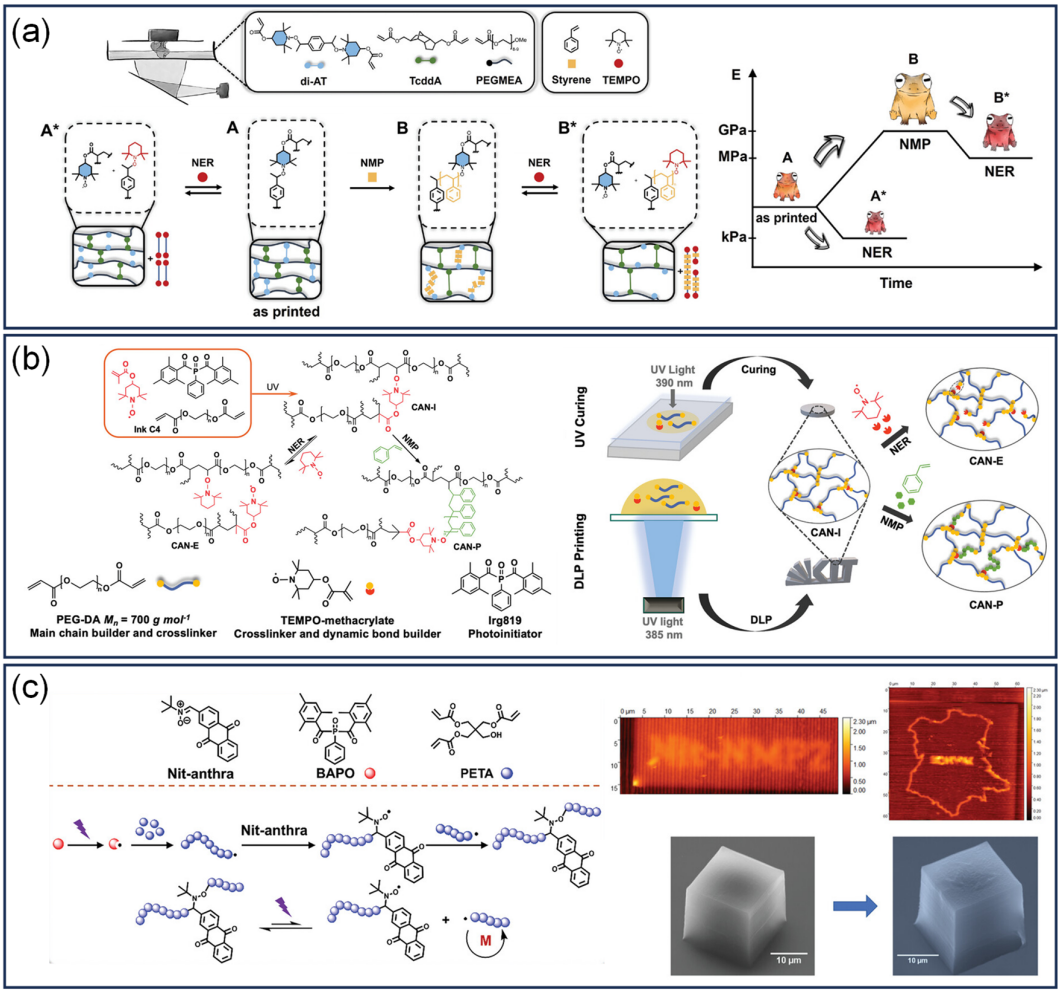


Figure 9. (**a**) The mechanism of adaptable polymer network based on the nitroxide exchange reaction (NER) and nitroxide-mediated polymerization (NMP) [118]. Copyright 2024, John Wiley and Sons. (**b**) The changes in polymer network influenced by NER and NMP, which affected the properties of the printed material [119]. Copyright 2024, John Wiley and Sons. (**c**) The modification of polymer network based on photochemical dissociation and nitroxide-mediated photopolymerization of alkoxyamine dynamic covalent bonds [120]. Copyright 2023, John Wiley and Sons.

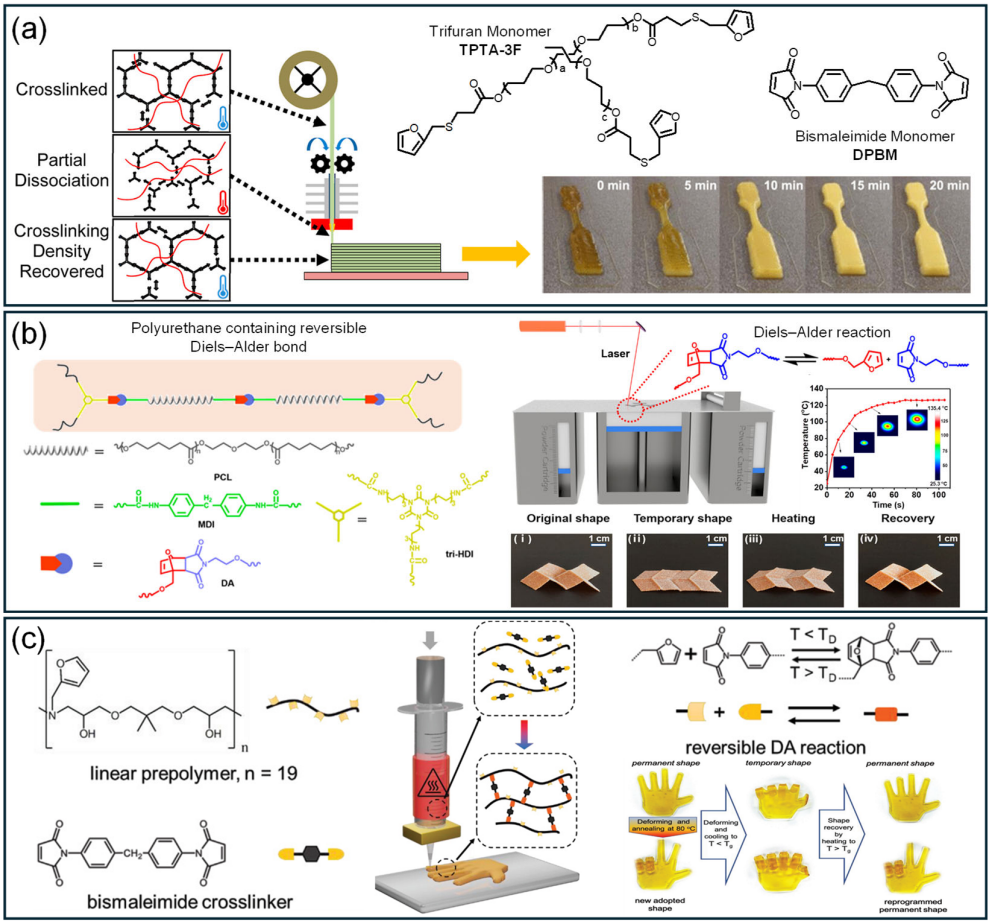


Figure 10. (**a**) The role of DA metathesis reaction in improving interlayers connection in 3D-printed pieces [124]. Copyright 2024, American Chemical Society. (**b**) The metathesis reaction of DC facilitating the infiltration of polymer into fillers during the SLS printing process [125]. Copyright 2022, American Chemical Society. (**c**) The introduction of DA bonds and their effects on variety of properties in the polymer network [126]. Copyright 2020, John Wiley and Sons.

3.3.2. Hindered Urea

Urea and urethane are stable linkages that serve as the primary building blocks for polyurethane networks. In contrast to urethane, urea is produced when an isocyanate reacts with a primary or secondary amine. Notably, hindered urea is regarded as a dynamic covalent bond. In hindered urea structures, the nitrogen atom is substituted with bulky groups such as tert-butyl, cyclohexyl, diisopropyl, or 2,6-diisopropyl aniline [127]. These bulky groups induce twisting of the C-N amide bond, which reduces n-π* conjugation and lowers the activation energy required for urea exchange or dissociation [128,129]. Urea linkages can also form intermolecular hydrogen bonds, making them unsuitable for the VPP printing process. In contrast, thermally induced 3D printing processes are enhanced by the metathesis of hindered urea bonds, while elevated temperatures cause hydrogen bonds to weaken.

The work conducted by Wang et al. is representative of 3D-printed polyurethane networks enabled by hindered urea chemistry as depicted in Figure 11a [130]. Exchange between hindered urea bonds imparts self-healing capabilities, consistent with other dynamic covalent materials. Polyurethanes generally exhibit a soft and stretchable nature compared to many other polymers. This flexibility was maintained post-printing, with the reported material capable of stretching to about 400% in all directions. The dynamic exchange of hindered urea groups also contributed to a reduction in Da. Enhanced softness further improved the self-healing performance of the printed material. In composite 3D

printing applications, a straightforward liquid-phase absorption method can be utilized, exemplified by the work of Li et al. (Figure 11b) [131]. Although CNTs were initially coated only on the surface of polymer powder particles, the printed polymer ultimately achieved homogeneous filler dispersion. As seen in prior studies on thermally induced DA printing, dissociation of hindered urea is central to these results. Moreover, CNT fillers impart electrical conductivity, expanding the potential for these materials to be used in advanced applications.

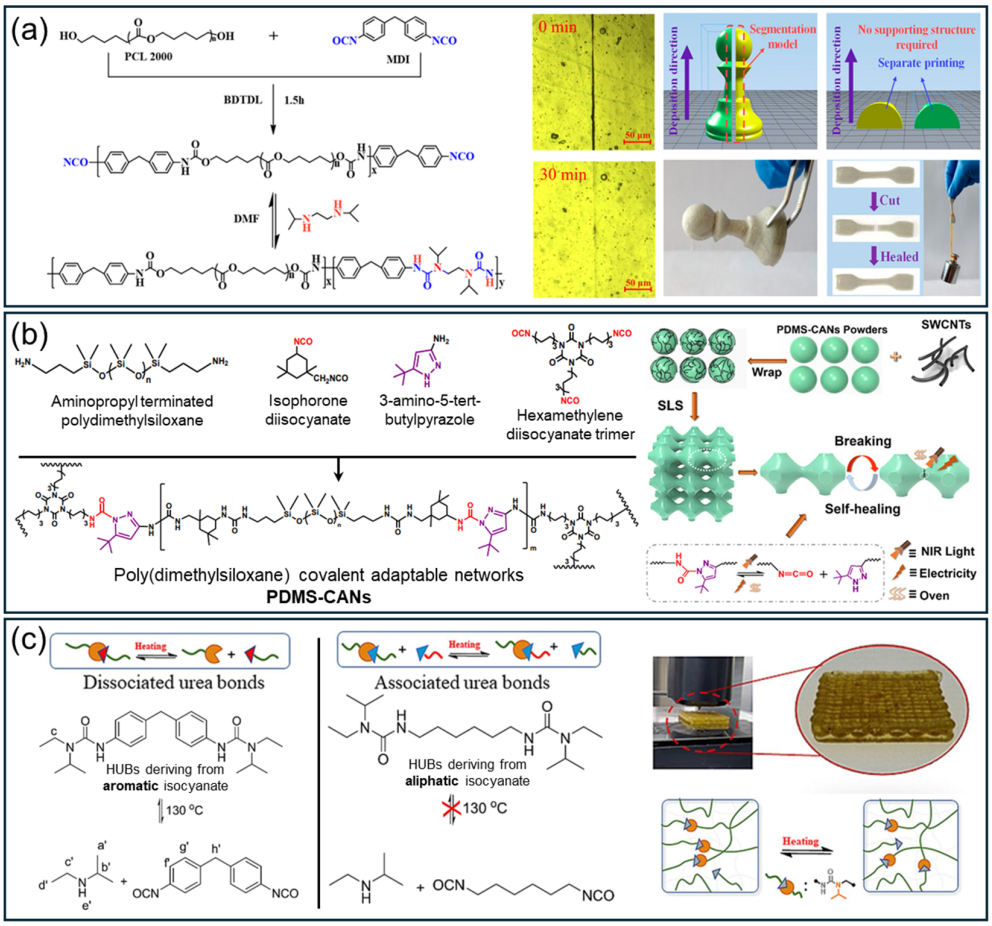


Figure 11. (**a**) Hindered urea dynamic covalent bonds in urethane used for 3D printing [130]. Copyright, 2021 American Chemical Society. (**b**) The role of hindered urea in simple processing of composite 3D printing [131]. Copyright, 2023 American Chemical Society. (**c**) The dissociative and associative urea bonds and their effects on properties and self-healing efficiency [132]. Copyright 2024, Elsevier.

As outlined in the study by Chen et al., the dynamic behavior of urea, whether dissociative or associative, is determined by the structure of the diisocyanate molecules (Figure 11c) [132]. Several factors influence whether the hindered urea acts as an associative (exchange reaction) or dissociative (retro reaction) dynamic covalent bond. Notably, aromatic and electron-withdrawing isocyanates are among the most effective at producing dissociative urea bonds [133,134]. The authors provided a clear perspective on how associative and dissociative mechanisms can impact the properties and self-healing efficiency of these materials. Ultimately, dissociative urea stands out as an excellent candidate for thermal-based 3D printing.

3.3.3. Transesterification

Transesterification, or ester exchange, is a dynamic covalent process central to many polymer networks. Although activating the exchange during printing typically requires elevated temperatures, the resulting covalent bonds afford the thermal and mechanical stability needed for particular printed items. In many systems, these bonds remain so robust that catalysts are often necessary to reduce the exchange temperature to within the operational range of the 3D printing process [135,136]. The use of catalysts is therefore crucial for facilitating reversible exchange at temperatures amenable to practical applications [137].

Reversible transesterification occurs predominantly through an associative mechanism. For this process to proceed, accessible nucleophiles must attack the ester, with hydroxyl groups being the most frequently utilized functionalities [138,139]. Several methods exist to introduce hydroxyl groups for this purpose. Joe et al. were the first to synthesize a polyurethane network with embedded ester linkages [140]. A secondary polymer featuring hydroxyl functionalities was then incorporated. In the presence of zinc acetylacetonate as a catalyst, the introduced hydroxyl groups engaged in exchange reactions with the esters (Figure 12a). Because the secondary chains introduced a high concentration of hydroxyl groups, the resulting material could be melted and processed by 3D printing. The dynamic exchange process also enabled self-healing and shape reprogramming capabilities.

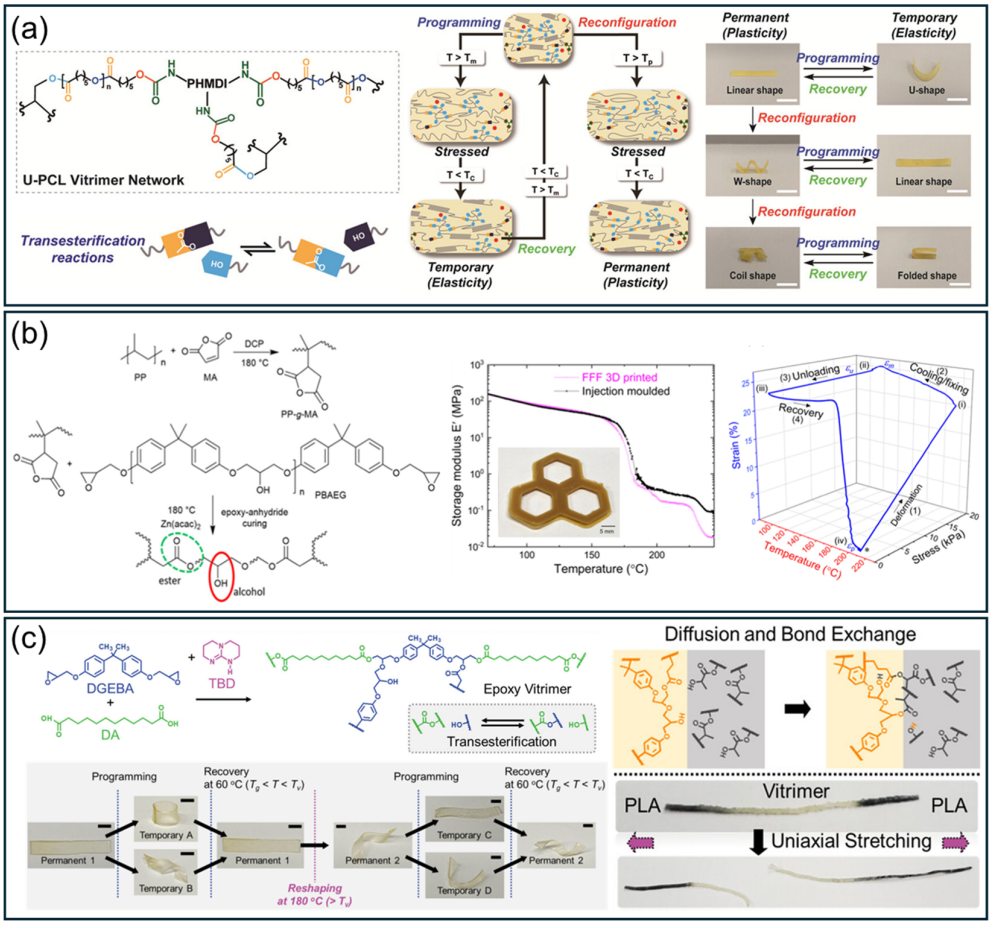


Figure 12. (**a**) Ester polymer network created from the esterification of two polymer chains through the transesterification reaction [140]. Copyright 2021, John Wiley and Sons. (**b**) The network containing ester bonds and hydroxyl functional groups that allow transesterification within the polymer itself [141]. Copyright, 2022 American Chemical Society. (**c**) The ester polymer network with variable hydroxyl concentration and controllable temperature-responsive properties [142]. Copyright 2021, John Wiley and Sons.

In a complementary approach, Kar et al. synthesized polymer chains by incorporating hydroxyl groups directly into the backbone (Figure 12b) [141]. Although the same catalyst was utilized, positioning hydroxyls within the main chain enhanced processability and facilitated the formation of a more homogeneous network with superior physical properties. Choi et al. also implemented this strategy, introducing additional hydroxyl groups into the network as demonstrated in Figure 12c [142]. Adjusting the molar ratio of the two monomers allowed precise control over the hydroxyl group content within the polymer. Consequently, both the physical properties and the temperature responsiveness of the material could be systematically modulated.

3.3.4. Imine Bonds

Imine bonds are readily formed between aldehyde and amine functional groups. He et al. developed an imine-containing network by reacting dialdehyde, diamine, and triamine monomers (Figure 13a) [143]. The thermally initiated metathesis reaction enabled efficient incorporation of multi-walled CNTs, which were then printed into the electrode component of an electronic device [144]. When the pure imine network was printed as the substrate and the composite as the conductive pathway, the chemical compatibility at their interface facilitated robust adhesion and conferred self-healing properties to the device.

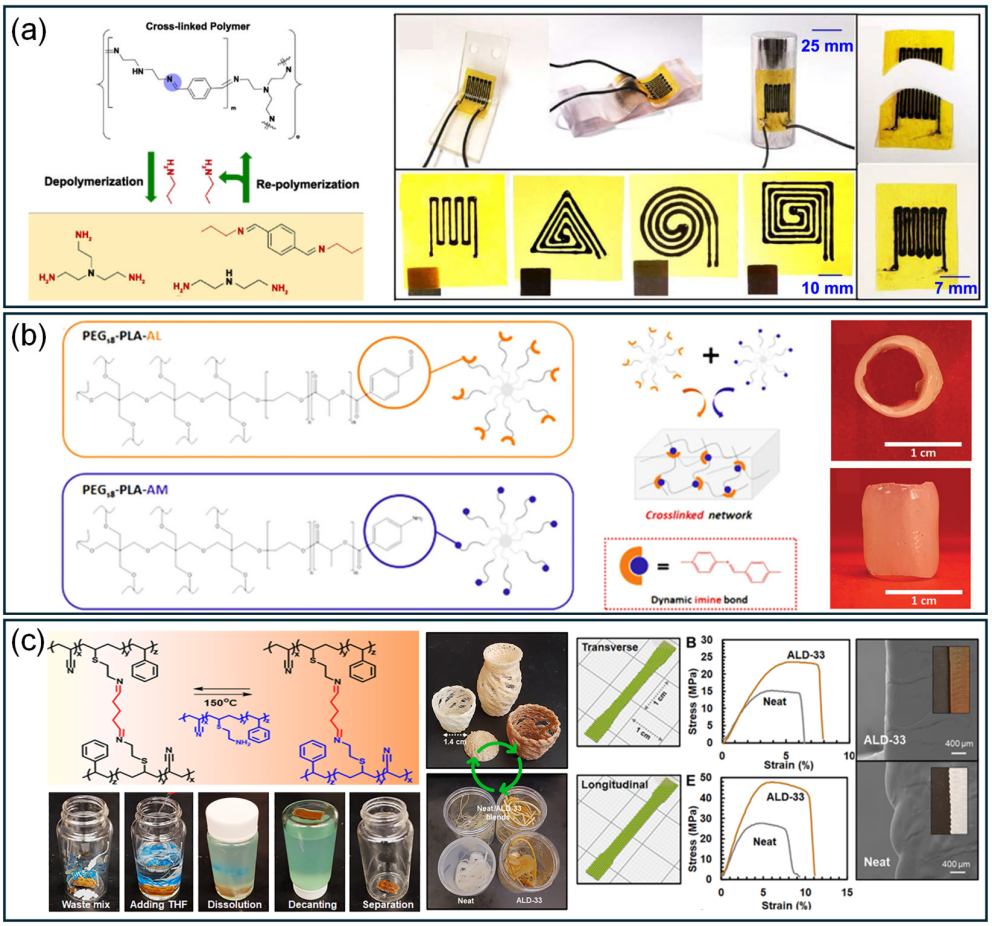


Figure 13. (**a**) Synthesis of an imine covalent bond-based network for 3D-printed self-healing electronic devices [143]. Copyright 2022, IOP Science. (**b**) Effects of water on the properties and self-healing of an imine-contained polymer network [145]. Copyright 2023, John Wiley and Sons. (**c**) The modification of commercially acrylonitrile–butadiene–styrene copolymer and the effects of imine crosslink concentrations [146]. Copyright 2022, Science.

Nonetheless, the propensity of imine bonds to undergo hydrolysis in the presence of water and humidity can impair material performance, as detailed by Grosjean et al. (Figure 13b) [145]. The study documented decreases in Young's modulus, stress at break, and strain at break under hydrated environments. Importantly, self-healing in the hydrated state also demonstrated diminished effectiveness compared to dry conditions. In contrast to hydrogel systems that rely on water for healing, here, water accelerates hydrolysis and alters the hydrolysis–condensation equilibrium such that bond-exchange is hindered. Thus, for practical use, stringent control of storage conditions and humidity is essential.

Kim et al. examined the influence of imine crosslink density on the properties of commercial acrylonitrile–butadiene–styrene (ABS) while retaining printability (Figure 13c) [146]. Primary amines were grafted onto ABS through a thiol–ene click reaction, which initially resulted in lower toughness and stress at break. As imine crosslinking increased, toughness and stress at break were restored and enhanced up to a certain limit, after which excessive crosslinking limited chain mobility and caused performance decline. This work demonstrates that incorporating dynamic covalent bonds into conventional polymers can enhance and tailor properties while maintaining compatibility with typical 3D printing processes.

3.3.5. Boronate–Ester Bonds

Peng et al. developed a network based on the metathesis reaction of the boronate–ester bond (Figure 14a) [147]. Self-healing was observed at approximately 100 °C for boronate–ester networks and at about 80 °C for boronate-anion systems. The extrusion process still required a nozzle temperature near 195 °C, which was ascribed to the substantial dynamic bond content and the thermal requirement for adequate bond dissociation and polymer flow. Nonetheless, the resulting materials exhibited robust self-healing, shape recovery, and shape reconfiguration.

Although boronate ester formation is straightforward, it proceeds slowly at low temperatures, including under ambient conditions. As a result, multiple groups incorporated additional, weaker interactions to rapidly stabilize the printed structure, providing sufficient time for the boronate ester to equilibrate and establish its network. This strategy facilitates injectability at 25 °C, making it particularly suitable for bio-related applications [148]. Once the boronate network is fully developed, the desired material properties can be more effectively imparted.

Building on this concept, Amaral et al. employed ionic-mediated sequential crosslinking with calcium chloride ($CaCl_2$) to create boronate-ester formulations suitable for 3D printing (Figure 14b) [149]. Although straightforward, the use of ions must be carefully controlled due to potential strong interactions with the surrounding environment, which vary depending on the ion type. Furthermore, boronate chemistry is inherently sensitive to pH, salt concentration, and the specific structure of diols [150]. Despite these challenges, the authors developed a boronate-ester network printable at 25 °C that enabled the encapsulation of living cells. In an alternative approach, Feng et al. utilized hydrogen bonding secondary polymer chains instead of ions (Figure 14c) [151]. Their dopamine-modified hyaluronic acid-based microgel ink was directly suitable for printing. Following deposition, ongoing formation of boronate-ester linkages contributed to further reinforcing the 3D construct, thereby offering a mild strategy that maintains both print precision and biocompatibility.

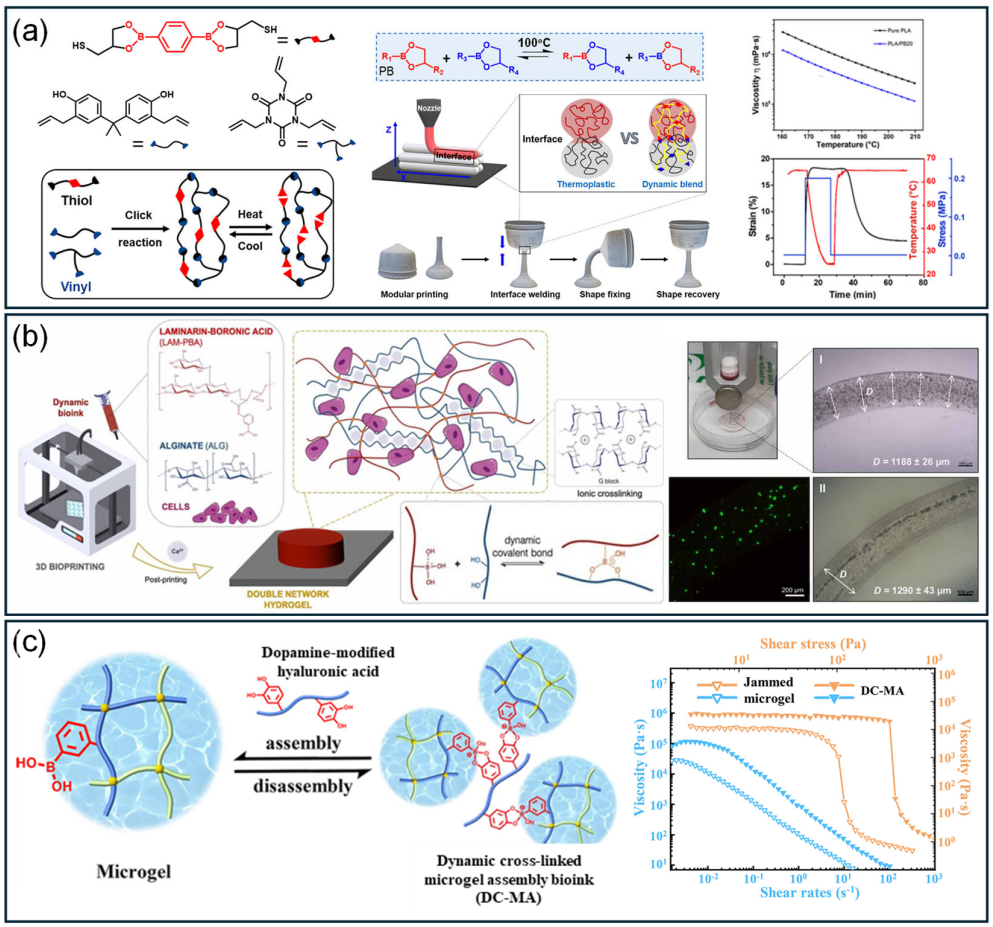


Figure 14. (**a**) Printable polymer network for fused deposition modeling based on metathesis reaction of boronate esters [147]. Copyright 2025, John Wiley and Sons. (**b**) Room-temperature printing of a polymer network containing boronate esters [149]. Copyright 2021, IOP Science. (**c**) Room-temperature 3D printing using a microgel material that contains dopamine-modified hyaluronic acid [151]. Copyright, 2022 American Chemical Society.

4. Application

4.1. Cell Culturing

While most non-hydrogel biocompatible polymers (e.g., polytetrafluoroethylene and silicone) are incompatible with current 3D printing processes, the inherent instability of numerous dynamic covalent linkages has also limited their application in long-term load-bearing implants such as knee arthroplasties. This might have been the reason why few studies have applied dynamic covalent bond-containing non-hydrogel polymers in biological applications. In contrast, hydrogels based on biocompatible polymers have been extensively studied for their superior cytocompatibility and aqueous processability [152–155]. Nevertheless, achieving reliable 3D printing of hydrogels is still a significant challenge: low solids content and soft mechanical properties can interfere with filament formation and structural integrity, the kinetics of gelation need careful tuning to balance cell viability, and successful post-deposition stabilization typically relies on optimized crosslink density and rapid viscoelastic recovery.

Although this approach has not yet been realized on a conventional 3D printer, Hull et al. demonstrated that dynamic covalent chemistry can be utilized to enhance hydrogel bioinks (Figure 15a) [156]. In their study, hyaluronan (hyaluronic acid, HA) was chemically modified into two forms, aldehyde and benzaldehyde, both of which reacted with hydrazine-modified elastin-like protein to form hydrazone bonds. Incorporating dual

hydrazone linkages resulted in improved printability and mechanical stability. Additionally, introducing a competitive molecule in the system allowed for tunable crosslinking density and reduced overall stiffness, while maintaining the inherent biocompatibility of HA. Tavakoli et al. further developed this concept by modifying HA to yield acetaldehyde and cysteine variants, as depicted in Figure 15b [157]. Their design employed two orthogonal dynamic reactions: disulfide formation via cysteine–cysteine coupling and thiazolidine formation originating from the reaction of cysteine with acetaldehyde. By adjusting the ratio between these modified forms of HA, the authors achieved tunable physical characteristics and printability. They also established that the resulting materials were suitable as cell culture scaffolds, providing evidence that dynamic exchange processes can be incorporated without adversely affecting cytocompatibility. Building on this approach, Lee et al. synthesized chondroitin sulfate derivatives capable of forming network structures linked by hydrazone bonds (Figure 15c) [158]. These materials exhibited shear-thinning characteristics, injectability, and self-healing capability. Furthermore, the inherent electrostatic charge of chondroitin sulfate was exploited to facilitate growth-factor loading and sustained release, supporting cell infiltration for use in regenerative medicine and tissue engineering applications.

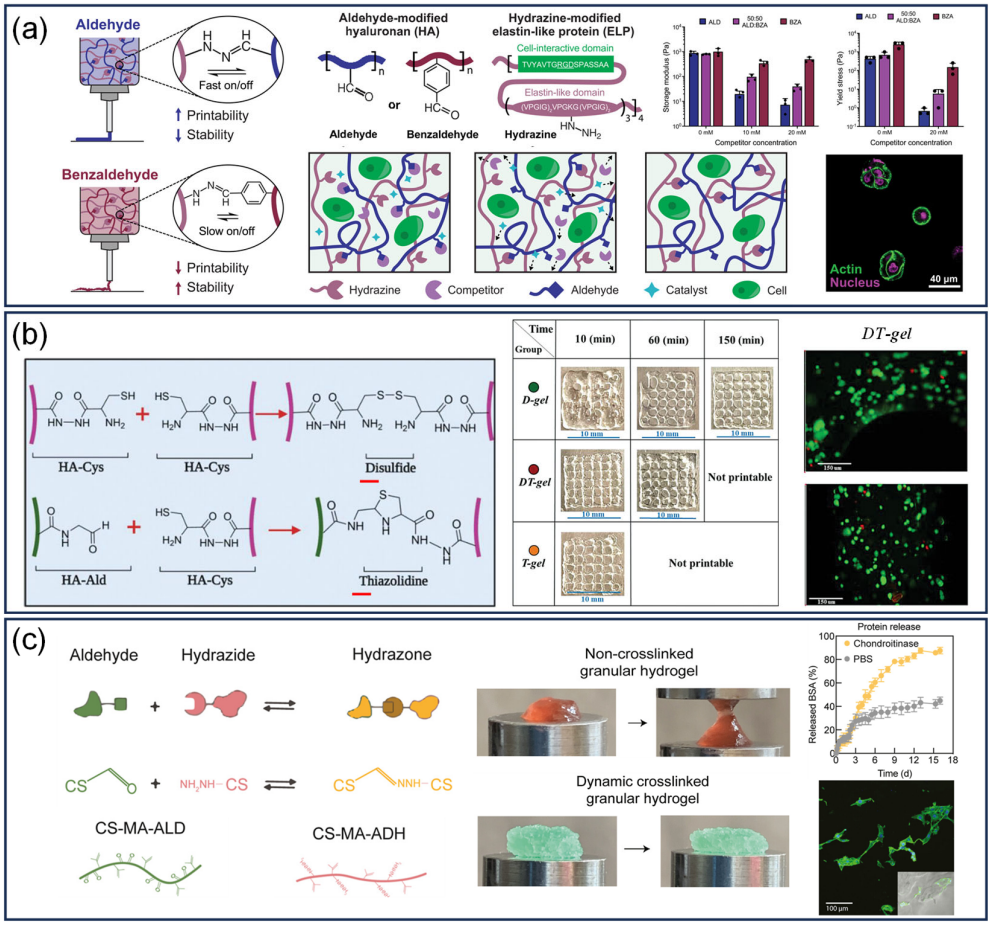


Figure 15. (**a**) Dual hydrazone dynamic covalent bonds built from aldehyde- and benzaldehyde-modified HAs for cell culturing [156]. Copyright 2023, Science. (**b**) Bioink of HA connected by disulfide–thiazolidine dual dynamic crosslinks for improving printability and stability [157]. Copyright 2023, John Wiley and Sons. (**c**) The modification of chondroitin sulfate for the introduction of hydrazone dynamic bonds [158]. Copyright, 2023 American Chemical Society.

4.2. Wound Dressing

As an extension of cell culture applications, 3D-printed polymer materials that utilize dynamic covalent bonds have strong potential for wound dressings. First, hydrogel materials have been shown to provide a moist environment that promotes wound healing [159]. Hydrogels derived from natural polymers are widely used in this area because of their biocompatibility [160]. However, gelatin-based and related hydrogels often have limited mechanical robustness, which prevents them from keeping pace with body motion and restricts their use. Introducing dynamic covalent bonds can help overcome this limitation by creating more stable crosslinking networks [161]. This effect was demonstrated by Zhang et al. (Figure 16a) [162]. Formation of imine bonds strengthened the coupling between hyaluronan (HA) and carboxymethyl chitosan, which in turn enabled more controlled degradation, improved swelling behavior, and enhanced adhesion.

On the other hand, 3D printing techniques allow materials to have structures that facilitate the wound healing process [163,164]. They also support patient-specific customization by matching the shape and size of the wound. For example, Joshi et al. used DLP printing to fabricate high-fidelity micro-pyramid structures (Figure 16b) [165]. These features acted as transient matrices that promoted diffusion and increased interfacial contact area, thereby improving adhesion. Meanwhile, Monavari et al. printed porous structures that were reported to encourage tissue regeneration and wound closure (Figure 16c) [166].

Although studies that combine both 3D printing and dynamic covalent chemistry remain limited, both approaches are already making clear contributions to wound healing materials. Their integration has strong potential to advance this application by uniting programmable mechanics, self-repair, and geometry-guided healing.

4.3. Soft Robotics

Dynamic covalent bonds are highly compatible with soft robotics applications [167,168]. High-frequency actuation places materials under persistent risk of defect formation and mechanical failure, a challenge that polymers with dynamic covalent linkages address through ongoing bond-exchange processes. Furthermore, exploiting intrinsic self-healing mechanisms offers a practical method for bonding components, which is critical in manufacturing soft robotic assemblies [169–171]. Numerous studies have also established that both shape recovery and shape reprogramming are foundational to the operational performance of soft robotic arms [172–174]. Therefore, the integration of 3D printing technologies with dynamic covalent chemistry enables the development of versatile platforms for advanced research in soft robotic systems.

Gomez et al. employed thioether-containing dynamic crosslinks and their associated exchange reactions to fabricate materials specifically for soft robotic applications (Figure 17a) [175]. Their research established that polymer networks with dynamic bonds facilitate the assembly of multiple 3D-printed components into intricate structures. The incorporation of bond-exchange mechanisms strengthened the interfacial connections, resulting in a network system that was significantly more stable than those based on hydrogen bonding. In addition to shape recovery and programmable deformation, the authors succeeded in constructing an entire robotic arm using these polymers, even though the individual parts differed in monomer composition and bulk characteristics. Yu et al. demonstrated the use of shape reprogramming as a means to simultaneously alter the physical properties of polymer samples (Figure 17b) [176]. When subjected to external stress, chain rearrangements induced by deformation caused substantial changes in network properties; subsequent thermal activation then fixed the newly programmed shape and permanently established the altered characteristics.

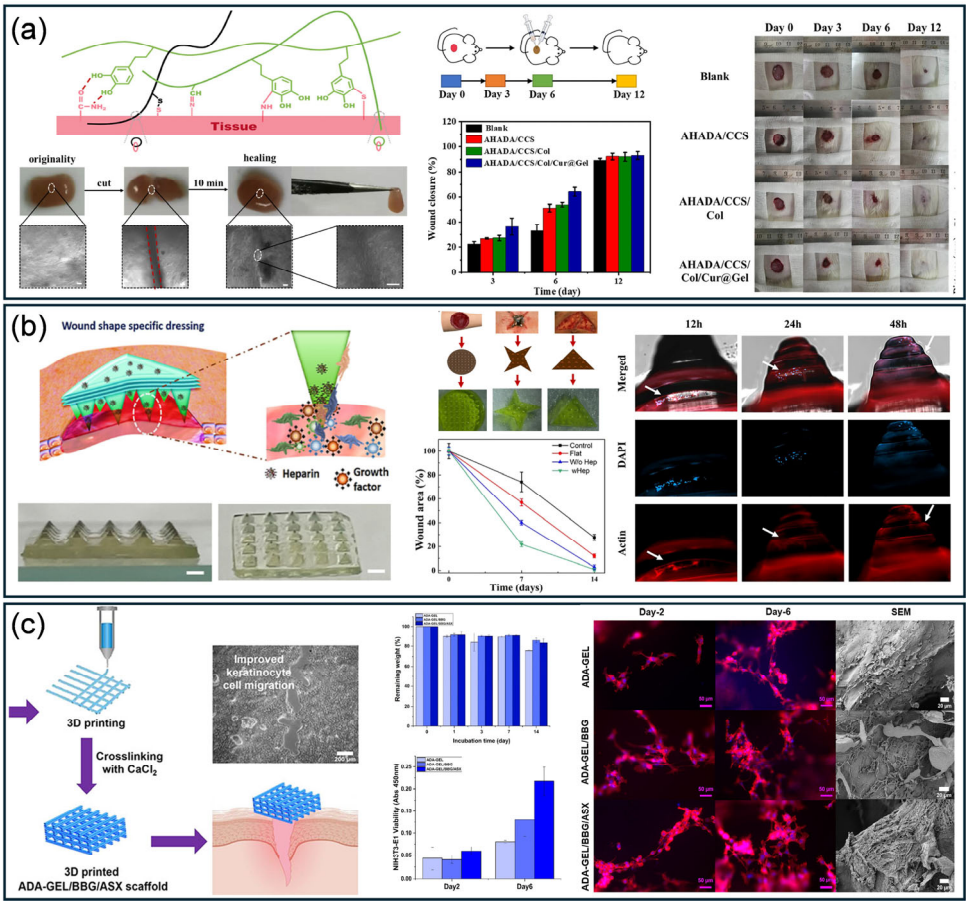


Figure 16. (**a**) Hyaluronic acid/carboxymethyl chitosan matrix connected through imine dynamic covalent bonds for wound dressing applications [162]. Copyright, 2023 American Chemical Society. (**b**) Micro-pyramid structure fabricated through 3D printing techniques that facilitate wound healing process [165]. Copyright, 2023 American Chemical Society. (**c**) Porous structure that has the ability to promote wound healing [166]. Copyright, 2023 American Chemical Society.

Despite these favorable characteristics, polymeric materials encounter persistent limitations in soft robotic applications. Incorporating magnetic fillers, as demonstrated by Zhu et al., enables composites to respond to external magnetic fields, allowing for more sophisticated actuation and control strategies (Figure 17c) [177]. As the network was assembled from monomers connected via imine bonds, self-healing and reprocessing occurred without notable interference from the fillers. Although the device was produced by laser cutting rather than 3D printing, the concept remains pertinent and should be considered for future printed soft robotic designs.

4.4. Tactile Sensor

Sensitivity, a primary performance metric for tactile sensors, is substantially improved when the sensing layers are designed with 3D microstructures [178,179]. Because device operation depends on deformation under applied force, self-healing capabilities are also highly desirable in sensing layers. Thus, polymers containing dynamic covalent bonds and compatible with 3D printing are of significant interest. When acting as active layers in capacitive tactile sensors or nanogenerators, polymers need to possess either a high dielectric permittivity or function as suitable hosts for organic salts/ionic liquids [180,181]. In contrast, resistive tactile sensors require the sensing material to be electrically conductive. Nonetheless, the inherent reversibility of dynamic bonds can compromise struc-

tural stability, especially when such bonds are employed in delicate, high-surface-area-printed architectures.

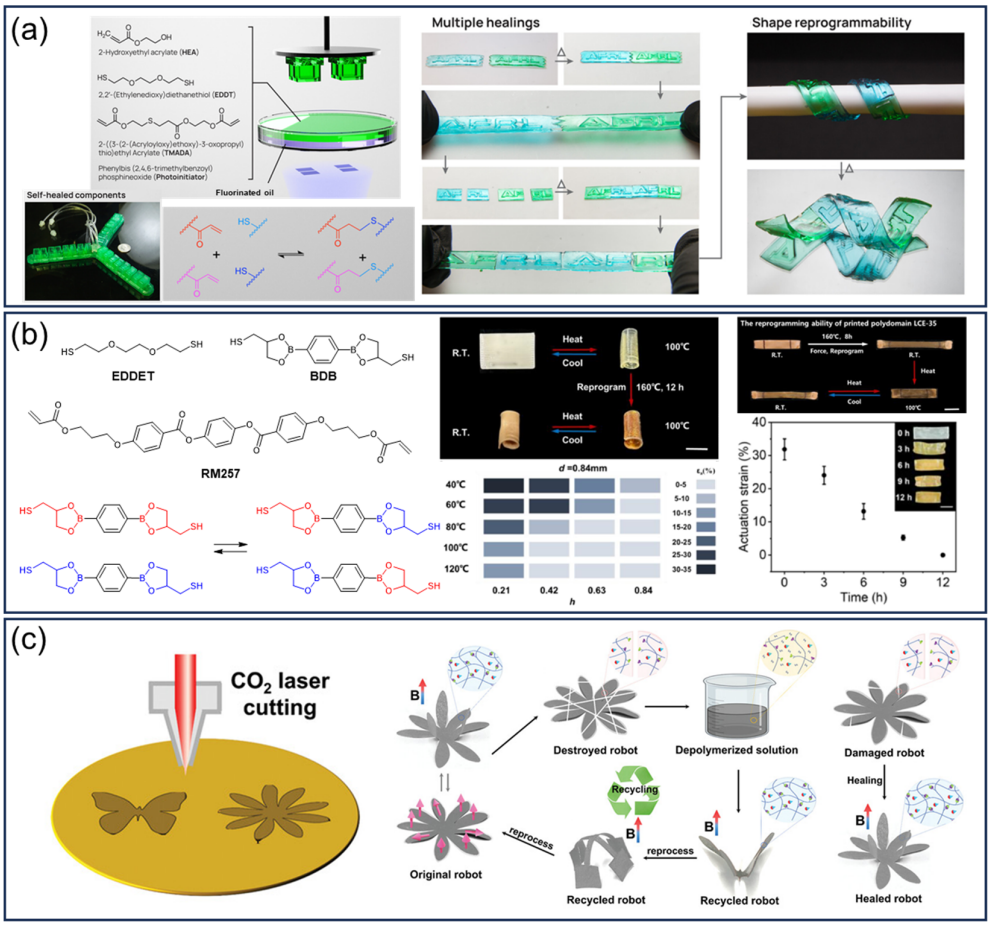


Figure 17. (**a**) Polymer containing dynamic covalent bond used to craft multiple pieces for application in soft robotics [175]. Copyright, 2021 American Chemical Society. (**b**) Reprogramming physical properties of a dynamic polymer network using heat treatment [176]. Copyright 2024, Elsevier. (**c**) Soft robotics built from a composite polymer containing imine dynamic bonds [177]. Copyright 2023, John Wiley and Sons.

Smith-Jones et al. developed modular 3D-printed components by incorporating butyl–vinyl imidazolium bis(trifluoromethanesulfonyl)imide ([BVIM][TFSI]) (Figure 18a) [182]. Through bond-exchange (metathesis), these parts were assembled into diverse configurations, yielding materials that exhibited force-dependent electrical conductivity and demonstrated their potential for resistive sensing applications. In related research, Zhang et al. established a boronate ester dynamic network capable of reversible resistance changes in response to mechanical stimuli (Figure 18b) [183]. This sensor effectively detected signals produced during human motion, and the same formulation was also used in extrusion-based 3D printing, supporting the approach for developing 3D architectures for tactile sensing purposes. Building upon this strategy, Zhang et al. reported a printed 3D structure containing the ionic liquid 1-ethyl-3-methylimidazolium bis(trifluoromethylsulfonyl)imide ([EMIM][TFSI]) (Figure 18c) [184]. The introduction of disulfide bonds provided the network with self-healing capability; although very intricate and delicate features limited complete recovery, the design still enabled high sensitivity in resistive tactile sensors. Furthermore, the associated thin-film material served efficiently as a dielectric layer in a triboelectric nanogenerator, highlighting the adaptability of dynamic bond-containing polymers for diverse sensing functionalities.

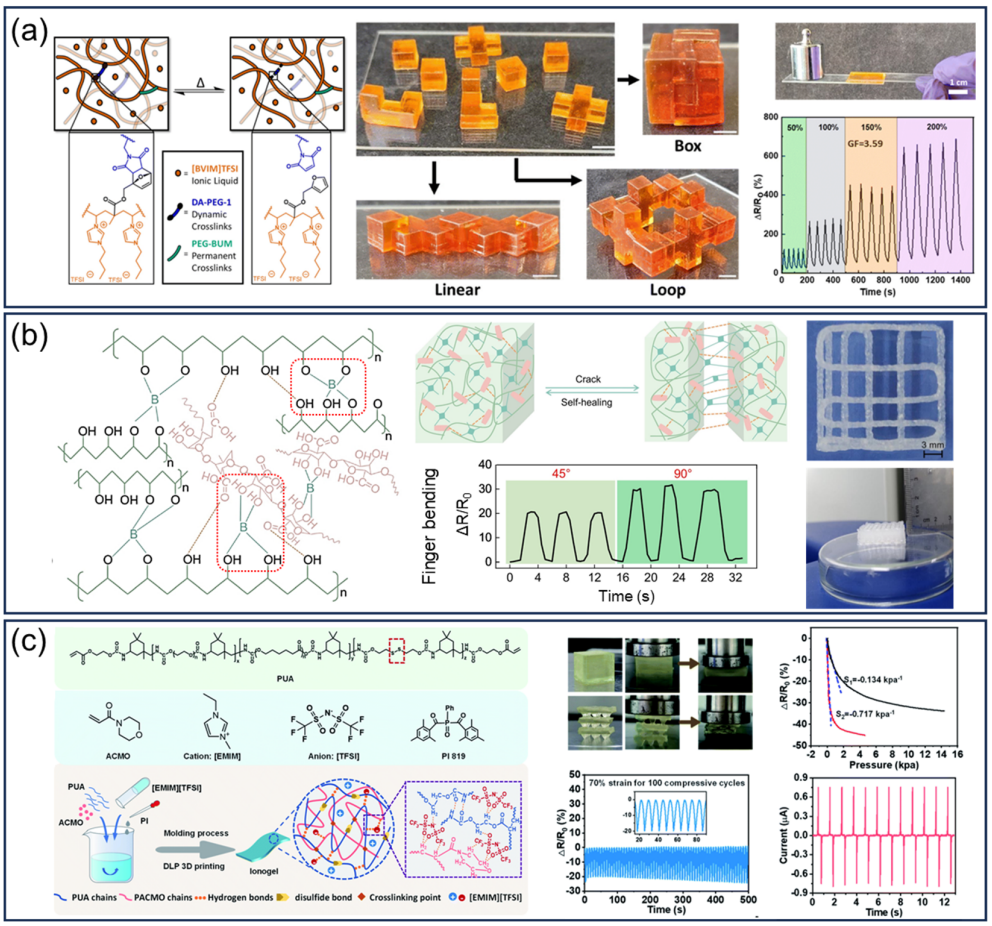


Figure 18. (**a**) Small 3D-printed dynamic polymer pieces that can assemble and function as resistive tactile sensor [182]. Copyright, 2024 Royal Society of Chemical. (**b**) Printable polymer gel for the resistive tactile sensor in recording body motion [183]. Copyright, 2022 Elsevier. (**c**) 3D dynamic polymer network structure containing ionic liquid [EMIM][TFSI] for resistive tactile sensor and triboelectric nanogenerator [184]. Copyright, 2022 Royal Society of Chemical.

5. Conclusions

Dynamic covalent bonds have been incorporated into polymer materials using various strategies. The incorporation of these bonds has bought about material multiple advantageous effects on the materials. (1) Firstly, the metathesis reaction of dynamic covalent bonds enables self-healing and reprocessing abilities of materials. (2) Secondly, the modified functional groups influence a variety of material properties due to their unique properties and chemical structures. (3) Finally, the introduction of dynamic covalent bonds helps overcome the limitation of anisotropy, which is a usual disadvantage of 3D printing.

Extensive investigations have demonstrated that printed objects can achieve high resolution and robust performance, emphasizing the substantial promise of these materials, especially with ongoing progress in 3D printing techniques. This review has also provided a concise overview of possible applications for 3D-printed polymers containing dynamic covalent bonds. However, despite these strengths, bond-exchange (metathesis) may present limitations in certain applications. Although soft robotic devices have utilized dynamic covalent networks with significant success, further research is necessary to broaden their application in other fields, particularly in biology and advanced sensors, where persistent challenges include stability, long-term performance, and processing limitations. As stability is currently the main limitation of materials containing dynamic covalent bonds, improving such aspects can be the center of future developments. Such improvements would not

only improve outcome performance of the materials but also significantly extend their field of applications.

Author Contributions: Conceptualization, T.D.N. and J.S.L.; writing—original draft preparation, T.D.N. and M.T.N.N.; writing—review and editing, T.D.N. and J.S.L.; supervision, J.S.L.; funding acquisition, J.S.L. All authors have read and agreed to the published version of the manuscript.

Funding: This work was supported by the National Research Foundation of Korea (NRF) grant funded by the Korea government (MSIT) (no. NRF2021R1F1A1053291).

Institutional Review Board Statement: Not applicable.

Informed Consent Statement: Not applicable.

Data Availability Statement: Not applicable.

Conflicts of Interest: The authors declare no conflicts of interest.

References

1. Kodama, H. Automatic method for fabricating a three-dimensional plastic model with photo-hardening polymer. *Rev. Sci. Instrum.* **1981**, *52*, 1770–1773.
2. Kumar, S. Selective laser sintering: A qualitative and objective approach. *JOM* **2003**, *55*, 43–47. [CrossRef]
3. Pagac, M.; Hajnys, J.; Ma, Q.-P.; Jancar, L.; Jansa, J.; Stefek, P.; Mesicek, J. A Review of Vat Photopolymerization Technology: Materials, Applications, Challenges, and Future Trends of 3D Printing. *Polymers* **2021**, *13*, 598. [CrossRef]
4. Ladani, L.; Sadeghilaridjani, M. Review of Powder Bed Fusion Additive Manufacturing for Metals. *Metals* **2021**, *11*, 1391. [CrossRef]
5. Ziaee, M.; Crane, N.B. Binder jetting: A review of process, materials, and methods. *Addit. Manuf.* **2019**, *28*, 781–801. [CrossRef]
6. Elkaseer, A.; Chen, K.J.; Janhsen, J.C.; Refle, O.; Hagenmeyer, V.; Scholz, S.G. Material jetting for advanced applications: A state-of-the-art review, gaps and future directions. *Addit. Manuf.* **2022**, *60*, 103270.
7. Dermeik, B.; Travitzky, N. Laminated Object Manufacturing of Ceramic-Based Materials. *Adv. Eng. Mater.* **2020**, *22*, 2000256. [CrossRef]
8. Ahn, D.-G. Directed Energy Deposition (DED) Process: State of the Art. *IJPEM-GT* **2021**, *8*, 703–742.
9. Voet, V.S.D. Closed-Loop Additive Manufacturing: Dynamic Covalent Networks in Vat Photopolymerization. *ACS Mater. Au* **2023**, *3*, 18–23. [CrossRef]
10. Zhu, G.; Houck, H.A.; Spiegel, C.A.; Selhuber-Unkel, C.; Hou, Y.; Blasco, E. Introducing Dynamic Bonds in Light-based 3D Printing. *Adv. Funct. Mater.* **2024**, *34*, 2300456.
11. Al Mousawi, A.; Poriel, C.; Dumur, F.; Toufaily, J.; Hamieh, T.; Fouassier, J.P.; Lalevée, J. Zinc Tetraphenylporphyrin as High Performance Visible Light Photoinitiator of Cationic Photosensitive Resins for LED Projector 3D Printing Applications. *Macromolecules* **2017**, *50*, 746–753. [CrossRef]
12. Zhang, J.; Lalevée, J.; Zhao, J.; Graff, B.; Stenzel, M.H.; Xiao, P. Dihydroxyanthraquinone derivatives: Natural dyes as blue-light-sensitive versatile photoinitiators of photopolymerization. *Polym. Chem.* **2016**, *7*, 7316–7324. [CrossRef]
13. Salas, A.; Zanatta, M.; Sans, V.; Roppolo, I. Chemistry in light-induced 3D printing. *ChemTexts* **2023**, *9*, 4. [CrossRef]
14. Ha, Y.M.; Choi, J.W.; Lee, S.H. Mass production of 3-D microstructures using projection microstereolithography. *J. Mech. Sci. Technol.* **2008**, *22*, 514–521. [CrossRef]
15. Choi, J.-W.; Wicker, R.; Lee, S.-H.; Choi, K.-H.; Ha, C.-S.; Chung, I. Fabrication of 3D biocompatible/biodegradable micro-scaffolds using dynamic mask projection microstereolithography. *J. Mater. Process. Technol.* **2009**, *209*, 5494–5503. [CrossRef]
16. Zhang, F.; Zhu, L.; Li, Z.; Wang, S.; Shi, J.; Tang, W.; Li, N.; Yang, J. The recent development of vat photopolymerization: A review. *Addit. Manuf.* **2021**, *48*, 102423. [CrossRef]
17. Afridi, A.; Al Rashid, A.; Koç, M. Recent advances in the development of stereolithography-based additive manufacturing processes: A review of applications and challenges. *Bioprinting* **2024**, *43*, e00360. [CrossRef]
18. Kang, J.-H.; Sakthiabirami, K.; Kim, H.-A.; Hosseini Toopghara, S.A.; Jun, M.-J.; Lim, H.-P.; Park, C.; Yun, K.-D.; Park, S.-W. Effects of UV Absorber on Zirconia Fabricated with Digital Light Processing Additive Manufacturing. *Materials* **2022**, *15*, 8726. [CrossRef]
19. Rooney, L.M.; Christopher, J.; Watson, B.; Kumar, Y.S.; Copeland, L.; Walker, L.D.; Foylan, S.; Amos, W.B.; Bauer, R.; McConnell, G. Printing, Characterizing, and Assessing Transparent 3D Printed Lenses for Optical Imaging. *Adv. Mater. Technol.* **2024**, *9*, 2400043. [CrossRef]

20. Zhang, H.; Maier, A.; Mathews, M.; Hu, J.; Zhao, X. Development of open-architecture two-wavelength grayscale digital light processing for advanced vat photopolymerization. *Addit. Manuf.* **2025**, *107*, 104818. [CrossRef]
21. Subedi, S.; Liu, S.; Wang, W.; Naser Shovon, S.M.A.; Chen, X.; Ware, H.O.T. Multi-material vat photopolymerization 3D printing: A review of mechanisms and applications. *npj Adv. Manuf.* **2024**, *1*, 9. [CrossRef]
22. Graça, A.; Bom, S.; Martins, A.M.; Ribeiro, H.M.; Marto, J. Vat-based photopolymerization 3D printing: From materials to topical and transdermal applications. *Asian J. Pharm. Sci.* **2024**, *19*, 100940. [CrossRef]
23. Maturi, M.; Locatelli, E.; Sanz de Leon, A.; Comes Franchini, M.; Molina, S.I. Sustainable approaches in vat photopolymerization: Advancements, limitations, and future opportunities. *Green Chem.* **2025**, *27*, 8710–8754. [CrossRef]
24. Song, C.; Zhao, Q.; Xie, T.; Wu, J. DLP 3D printing of electrically conductive hybrid hydrogels via polymerization-induced phase separation and subsequent in situ assembly of polypyrrole. *J. Mater. Chem. A* **2024**, *12*, 5348–5356. [CrossRef]
25. Dhand, A.P.; Kirkpatrick, B.E.; Garay-Sarmiento, M.; Nelson, B.R.; Miksch, C.E.; Meurer-Zeman, B.; Zlotnick, H.M.; Mandal, A.; Lee, J.S.; Cione, J.; et al. Digital light processing of photoresponsive and programmable hydrogels. *Sci. Adv.* **2025**, *11*, eadw9262. [CrossRef] [PubMed]
26. Xu, F.; Jin, H.; Wu, H.; Jiang, A.; Qiu, B.; Liu, L.; Gao, Q.; Lin, B.; Kong, W.; Chen, S.; et al. Digital light processing printed hydrogel scaffolds with adjustable modulus. *Sci. Rep.* **2024**, *14*, 15695. [CrossRef]
27. Mohammed, M.K.; Alahmari, A.; Alkhalefah, H.; Abidi, M.H. Evaluation of zirconia ceramics fabricated through DLP 3d printing process for dental applications. *Heliyon* **2024**, *10*, e36725. [CrossRef]
28. Huang, J.; Qin, Q.; Wang, J. A Review of Stereolithography: Processes and Systems. *Processes* **2020**, *8*, 1138. [CrossRef]
29. Farsari, M.; Chichkov, B.N. Two-photon fabrication. *Nat. Photonics* **2009**, *3*, 450–452. [CrossRef]
30. Takada, K.; Sun, H.-B.; Kawata, S. Improved spatial resolution and surface roughness in photopolymerization-based laser nanowriting. *Appl. Phys. Lett.* **2005**, *86*, 071122. [CrossRef]
31. Yan, Y.-X.; Tao, X.-T.; Sun, Y.-H.; Xu, G.-B.; Wang, C.-K.; Yang, J.-X.; Zhao, X.; Wu, Y.-Z.; Ren, Y.; Jiang, M.-H. Two new asymmetrical two-photon photopolymerization initiators: Synthesis, characterization and nonlinear optical properties. *Opt. Mater.* **2005**, *27*, 1787–1792. [CrossRef]
32. Arif, Z.U.; Khalid, M.Y.; Tariq, A.; Hossain, M.; Umer, R. 3D printing of stimuli-responsive hydrogel materials: Literature review and emerging applications. *Giant* **2024**, *17*, 100209. [CrossRef]
33. Wang, X.; Liu, J.; Zhang, Y.; Kristiansen, P.M.; Islam, A.; Gilchrist, M.; Zhang, N. Advances in precision microfabrication through digital light processing: System development, material and applications. *Virtual Phys. Prototyp.* **2023**, *18*, e2248101. [CrossRef]
34. Caplins, B.W.; Higgins, C.I.; Kolibaba, T.J.; Arp, U.; Miller, C.C.; Poster, D.L.; Zarobila, C.J.; Zong, Y.; Killgore, J.P. Characterizing light engine uniformity and its influence on liquid crystal display based vat photopolymerization printing. *Addit. Manuf.* **2023**, *62*, 103381. [CrossRef]
35. Liu, S.; Borjigin, T.; Schmitt, M.; Morlet-Savary, F.; Xiao, P.; Lalevée, J. High-Performance Photoinitiating Systems for LED-Induced Photopolymerization. *Polymers* **2023**, *15*, 342. [CrossRef]
36. Chaudhary, R.; Fabbri, P.; Leoni, E.; Mazzanti, F.; Akbari, R.; Antonini, C. Additive manufacturing by digital light processing: A review. *Prog. Addit. Manuf.* **2023**, *8*, 331–351.
37. Beluze, L.; Bertsch, A.; Renaud, P. Microstereolithography: A new process to build complex 3D objects. In *Design, Test, and Microfabrication of MEMS and MOEMS*; SPIE: Bellingham, WA, USA, 1999; pp. 808–817.
38. Alparslan, C.; Bayraktar, Ş. Advances in Digital Light Processing (DLP) Bioprinting: A Review of Biomaterials and Its Applications, Innovations, Challenges, and Future Perspectives. *Polymers* **2025**, *17*, 1287. [CrossRef] [PubMed]
39. Nam, J.; Kim, M. Advances in materials and technologies for digital light processing 3D printing. *Nano Converg.* **2024**, *11*, 45. [CrossRef]
40. Paral, S.K.; Lin, D.-Z.; Cheng, Y.-L.; Lin, S.-C.; Jeng, J.-Y. A Review of Critical Issues in High-Speed Vat Photopolymerization. *Polymers* **2023**, *15*, 2716. [CrossRef]
41. Zhan, S.; Guo, A.X.Y.; Cao, S.C.; Liu, N. 3D Printing Soft Matters and Applications: A Review. *Int. J. Mol. Sci.* **2022**, *23*, 3790. [CrossRef]
42. Truby, R.L.; Lewis, J.A. Printing soft matter in three dimensions. *Nature* **2016**, *540*, 371–378. [CrossRef] [PubMed]
43. Tuli, N.T.; Khatun, S.; Rashid, A.B. Unlocking the future of precision manufacturing: A comprehensive exploration of 3D printing with fiber-reinforced composites in aerospace, automotive, medical, and consumer industries. *Heliyon* **2024**, *10*, e27328. [CrossRef] [PubMed]
44. Park, S.; Shou, W.; Makatura, L.; Matusik, W.; Fu, K. 3D printing of polymer composites: Materials, processes, and applications. *Matter* **2022**, *5*, 43–76. [CrossRef]
45. Memon, H.; Wei, Y.; Zhu, C. Correlating the thermomechanical properties of a novel bio-based epoxy vitrimer with its crosslink density. *Mater. Today Commun.* **2021**, *29*, 102814. [CrossRef]
46. Jia, Y.; Ying, H.; Zhang, Y.; He, H.; Cheng, J. Reconfigurable Poly(urea-urethane) Thermoset Based on Hindered Urea Bonds with Triple-Shape-Memory Performance. *Macromol. Chem. Phys.* **2019**, *220*, 1900148. [CrossRef]

47. Snyder, R.L.; Fortman, D.J.; De Hoe, G.X.; Hillmyer, M.A.; Dichtel, W.R. Reprocessable Acid-Degradable Polycarbonate Vitrimers. *Macromolecules* **2018**, *51*, 389–397. [CrossRef]
48. Shi, Q.; Yu, K.; Kuang, X.; Mu, X.; Dunn, C.K.; Dunn, M.L.; Wang, T.; Qi, H.J. Recyclable 3D printing of vitrimer epoxy. *Mater. Horiz.* **2017**, *4*, 598–607. [CrossRef]
49. Wickramasinghe, S.; Manalo, A.; Alajarmeh, O.; Sorbello, C.D.; Weerakoon, S.; Ngo, T.D.; Benmokrane, B. Advancing polymer composites in civil infrastructure through 3D printing. *Autom. Constr.* **2025**, *177*, 106311. [CrossRef]
50. Fang, Z.; Shi, Y.; Mu, H.; Lu, R.; Wu, J.; Xie, T. 3D printing of dynamic covalent polymer network with on-demand geometric and mechanical reprogrammability. *Nat. Commun.* **2023**, *14*, 1313. [CrossRef]
51. Liang, T.; Cai, Y.; Zhou, L.; Zang, T.; Wu, L.; Fei, G.; Cardon, L.; Xia, H. External field induced high speed sintering of dynamically cross-linked polydimethylsiloxane: Mechanical properties and electromagnetic wave absorption. *Addit. Manuf.* **2025**, *109*, 104860. [CrossRef]
52. Cook, A.L.; Dearborn, M.A.; Anderberg, T.M.; Vaidya, K.; Jureller, J.E.; Esser-Kahn, A.P.; Squires, A.H. Polymer Patterning by Laser-Induced Multipoint Initiation of Frontal Polymerization. *ACS Appl. Mater. Interfaces* **2024**, *16*, 17973–17980. [CrossRef] [PubMed]
53. Mejia, E.B.; McDougall, L.; Gonsalves, N.; Darby, D.R.; Greenlee, A.J.; Commisso, A.; Johnson, J.A.; Sottos, N.; Appelhans, L.N.; Cook, A.W.; et al. Real-time process monitoring and automated control for direct ink write 3D printing of frontally polymerizing thermosets. *npj Adv. Manuf.* **2025**, *2*, 18. [PubMed]
54. Bai, W.; Zhang, X.; Gao, C.; Zhao, X.; He, Y.; Shang, Y.; Shi, B.; Lu, L.; Chu, D. 3D printing of CNTs-modified continuous carbon fiber composites driven by Joule-heat resin curing. *Int. J. Therm. Sci.* **2025**, *216*, 110048. [CrossRef]
55. Hales, S.; Tokita, E.; Neupane, R.; Ghosh, U.; Elder, B.; Wirthlin, D.; Kong, Y.L. 3D printed nanomaterial-based electronic, biomedical, and bioelectronic devices. *Nanotechnology* **2020**, *31*, 172001. [CrossRef]
56. Pranzo, D.; Larizza, P.; Filippini, D.; Percoco, G. Extrusion-Based 3D Printing of Microfluidic Devices for Chemical and Biomedical Applications: A Topical Review. *Micromachines* **2018**, *9*, 374. [CrossRef]
57. Cuan-Urquizo, E.; Barocio, E.; Tejada-Ortigoza, V.; Pipes, R.B.; Rodriguez, C.A.; Roman-Flores, A. Characterization of the Mechanical Properties of FFF Structures and Materials: A Review on the Experimental, Computational and Theoretical Approaches. *Materials* **2019**, *12*, 895. [CrossRef]
58. Deng, X.; Zeng, Z.; Peng, B.; Yan, S.; Ke, W. Mechanical Properties Optimization of Poly-Ether-Ether-Ketone via Fused Deposition Modeling. *Materials* **2018**, *11*, 216. [CrossRef]
59. Wang, L.; Gramlich, W.M.; Gardner, D.J. Improving the impact strength of Poly(lactic acid) (PLA) in fused layer modeling (FLM). *Polymer* **2017**, *114*, 242–248. [CrossRef]
60. Li, C.; Feng, C.; Zhang, L.; Zhang, L.; Wang, L. Direct ink writing of polymer-based materials—A review. *Polym. Eng. Sci.* **2025**, *65*, 431–454. [CrossRef]
61. Jia, Y.; Xie, H.; Qian, J.; Zhang, Y.; Zheng, H.; Wei, F.; Li, Y.; Zhao, Z. Recent Progress on the 3D Printing of Dynamically Cross-Linked Polymers. *Adv. Funct. Mater.* **2024**, *34*, 2307279. [CrossRef]
62. Guo, Y.; Chen, S.; Sun, L.; Yang, L.; Zhang, L.; Lou, J.; You, Z. Degradable and Fully Recyclable Dynamic Thermoset Elastomer for 3D-Printed Wearable Electronics. *Adv. Funct. Mater.* **2021**, *31*, 2009799. [CrossRef]
63. Kim, M.; Nian, S.; Rau, D.A.; Huang, B.; Zhu, J.; Freychet, G.; Zhernenkov, M.; Cai, L.-H. 3D Printable Modular Soft Elastomers from Physically Cross-linked Homogeneous Associative Polymers. *ACS Polym. Au* **2024**, *4*, 98–108. [CrossRef]
64. Shi, S.; Jiang, Y.; Ren, H.; Deng, S.; Sun, J.; Cheng, F.; Jing, J.; Chen, Y. 3D-Printed Carbon-Based Conformal Electromagnetic Interference Shielding Module for Integrated Electronics. *Nano-Micro Lett.* **2024**, *16*, 85. [CrossRef]
65. Solís Pinargote, N.W.; Smirnov, A.; Peretyagin, N.; Seleznev, A.; Peretyagin, P. Direct Ink Writing Technology (3D Printing) of Graphene-Based Ceramic Nanocomposites: A Review. *Nanomaterials* **2020**, *10*, 1300. [CrossRef] [PubMed]
66. Saadi, M.A.S.R.; Maguire, A.; Pottackal, N.T.; Thakur, M.S.H.; Ikram, M.M.; Hart, A.J.; Ajayan, P.M.; Rahman, M.M. Direct Ink Writing: A 3D Printing Technology for Diverse Materials. *Adv. Mater.* **2022**, *34*, 2108855. [CrossRef] [PubMed]
67. Tabriz, A.G.; Kuofie, H.; Scoble, J.; Boulton, S.; Douroumis, D. Selective Laser Sintering for printing pharmaceutical dosage forms. *J. Drug Deliv. Sci.* **2023**, *86*, 104699. [CrossRef]
68. Lekurwale, S.; Karanwad, T.; Banerjee, S. Selective laser sintering (SLS) of 3D printlets using a 3D printer comprised of IR/red-diode laser. *Ann. 3D Print. Med.* **2022**, *6*, 100054. [CrossRef]
69. Rastogi, P.; Gharde, S.; Kandasubramanian, B. Thermal Effects in 3D Printed Parts. In *3D Printing in Biomedical Engineering*; Singh, S., Prakash, C., Singh, R., Eds.; Springer: Singapore, 2020; pp. 43–68.
70. Tel, A.; Kornfellner, E.; Molnár, E.; Johannes, S.; Moscato, F.; Robiony, M. Selective laser sintering at the Point-of-Care 3D printing laboratory in hospitals for cranio-maxillo-facial surgery: A further step into industrial additive manufacturing made available to clinicians. *Ann. 3D Print. Med.* **2024**, *16*, 100175. [CrossRef]
71. Yehia, H.M.; Hamada, A.; Sebaey, T.A.; Abd-Elaziem, W. Selective Laser Sintering of Polymers: Process Parameters, Machine Learning Approaches, and Future Directions. *J. Manuf. Mater. Process.* **2024**, *8*, 197. [CrossRef]

72. Olakanmi, E.O.; Cochrane, R.F.; Dalgarno, K.W. A review on selective laser sintering/melting (SLS/SLM) of aluminium alloy powders: Processing, microstructure, and properties. *Prog. Mater. Sci.* **2015**, *74*, 401–477. [CrossRef]
73. Xu, T.; Shen, W.; Lin, X.; Xie, Y.M. Mechanical Properties of Additively Manufactured Thermoplastic Polyurethane (TPU) Material Affected by Various Processing Parameters. *Polymers* **2020**, *12*, 3010. [CrossRef] [PubMed]
74. Stichel, T.; Frick, T.; Laumer, T.; Tenner, F.; Hausotte, T.; Merklein, M.; Schmidt, M. A Round Robin study for selective laser sintering of polymers: Back tracing of the pore morphology to the process parameters. *Mater. Process. Technol.* **2018**, *252*, 537–545. [CrossRef]
75. Morano, C.; Pagnotta, L. Additive manufactured parts produced by selective laser sintering technology: Porosity formation mechanisms. *J. Polym. Eng.* **2023**, *43*, 537–555. [CrossRef]
76. Denissen, W.; Winne, J.M.; Du Prez, F.E. Vitrimers: Permanent organic networks with glass-like fluidity. *Chem. Sci.* **2016**, *7*, 30–38. [CrossRef]
77. Marco-Dufort, B.; Iten, R.; Tibbitt, M.W. Linking Molecular Behavior to Macroscopic Properties in Ideal Dynamic Covalent Networks. *JACS* **2020**, *142*, 15371–15385. [CrossRef]
78. Wojtecki, R.J.; Meador, M.A.; Rowan, S.J. Using the dynamic bond to access macroscopically responsive structurally dynamic polymers. *Nat. Mater.* **2011**, *10*, 14–27. [CrossRef]
79. Elling, B.R.; Dichtel, W.R. Reprocessable Cross-Linked Polymer Networks: Are Associative Exchange Mechanisms Desirable? *ACS Cent. Sci.* **2020**, *6*, 1488–1496. [CrossRef]
80. Jang, S.; Hernandez Alvarez, E.I.; Chen, C.; Jing, B.B.; Shen, C.; Braun, P.V.; Schleife, A.; Schroeder, C.M.; Evans, C.M. Control of Lithium Salt Partitioning, Coordination, and Solvation in Vitrimer Electrolytes. *Chem. Mater.* **2023**, *35*, 8039–8049. [CrossRef]
81. Zohdi, N.; Yang, R. Material Anisotropy in Additively Manufactured Polymers and Polymer Composites: A Review. *Polymers* **2021**, *13*, 3368. [CrossRef]
82. Guessasma, S.; Belhabib, S.; Nouri, H.; Ben Hassana, O. Anisotropic damage inferred to 3D printed polymers using fused deposition modelling and subject to severe compression. *Eur. Polym. J.* **2016**, *85*, 324–340. [CrossRef]
83. Hoff, B.W.; Maestas, S.S.; Hayden, S.C.; Harrigan, D.J.; Grudt, R.O.; Ostraat, M.L.; Horwath, J.C.; Leontsev, S. Dielectric strength heterogeneity associated with printing orientation in additively manufactured polymer materials. *Addit. Manuf.* **2018**, *22*, 21–30. [CrossRef]
84. Somireddy, M.; Czekanski, A. Anisotropic material behavior of 3D printed composite structures—Material extrusion additive manufacturing. *Mater. Des.* **2020**, *195*, 108953. [CrossRef]
85. Shemelya, C.; De La Rosa, A.; Torrado, A.R.; Yu, K.; Domanowski, J.; Bonacuse, P.J.; Martin, R.E.; Juhasz, M.; Hurwitz, F.; Wicker, R.B.; et al. Anisotropy of thermal conductivity in 3D printed polymer matrix composites for space based cube satellites. *Addit. Manuf.* **2017**, *16*, 186–196. [CrossRef]
86. Liguori, A.; Kalita, N.K.; Adamus, G.; Kowalczuk, M.; Focarete, M.L.; Hakkarainen, M. Bio-based ester- and ester-imine resins for digital light processing 3D printing: The role of the chemical structure on reprocessability and susceptibility to biodegradation under simulated industrial composting conditions. *Eur. Polym. J.* **2024**, *219*, 113384. [CrossRef]
87. Vilanova-Pérez, A.; De la Flor, S.; Fernández-Francos, X.; Serra, À.; Roig, A. Biobased Imine Vitrimers Obtained by Photo and Thermal Curing Procedures—Promising Materials for 3D Printing. *ACS Appl. Polym. Mater.* **2024**, *6*, 3364–3372. [CrossRef] [PubMed]
88. Liguori, A.; Oliva, E.; Sangermano, M.; Hakkarainen, M. Digital Light Processing 3D Printing of Isosorbide- and Vanillin-Based Ester and Ester–Imine Thermosets: Structure–Property Recyclability Relationships. *ACS Sustain. Chem. Eng.* **2023**, *11*, 14601–14613. [CrossRef] [PubMed]
89. Stouten, J.; Schnelting, G.H.M.; Hul, J.; Sijstermans, N.; Janssen, K.; Darikwa, T.; Ye, C.; Loos, K.; Voet, V.S.D.; Bernaerts, K.V. Biobased Photopolymer Resin for 3D Printing Containing Dynamic Imine Bonds for Fast Reprocessability. *ACS Appl. Mater. Interfaces* **2023**, *15*, 27110–27119. [CrossRef]
90. Nguyen, T.D.; Phan, T.T.T.; Lee, J.S. Fabrication and Characterization of Self-Healable Polydisulfide Network-Based Composites. *ACS Appl. Polym. Mater.* **2023**, *5*, 485–493. [CrossRef]
91. Montazerozohori, M.; Joohari, S.; Karami, B.; Haghighat, N. Fast and Highly Efficient Solid State Oxidation of Thiols. *Molecules* **2007**, *12*, 694–702. [CrossRef]
92. Sousa, J.R.L.; Franco, M.S.; Mendes, L.D.; Araújo, L.A.; Neto, J.S.S.; Frizon, T.E.A.; dos Santos, V.B.; Carasek, E.; Saba, S.; Rafique, J.; et al. KIO_3-catalyzed selective oxidation of thiols to disulfides in water under ambient conditions. *Org. Biomol. Chem.* **2024**, *22*, 2175–2181. [CrossRef]
93. Nguyen, M.T.N.; Nguyen, T.D.; Han, J.-H.; Lee, J.S. Synthesis of PDMS Chain Structure with Introduced Dynamic Covalent Bonding for High-Performance Rehealable Tactile Sensor Application. *Small Methods* **2024**, *8*, 2400163. [CrossRef]
94. Chen, J.; Jiang, S.; Gao, Y.; Sun, F. Reducing volumetric shrinkage of photopolymerizable materials using reversible disulfide-bond reactions. *J. Mater. Sci.* **2018**, *53*, 16169–16181. [CrossRef]

95. Nguyen, T.D.; Lee, J.S. Dynamic Bonds in Biopolymers: Enhancing Performance and Properties. *Polymers* **2025**, *17*, 457. [CrossRef] [PubMed]
96. Wang, S.; Yin, J.; Huang, W.; Ye, J.; Deng, H.; Huang, J.; Wang, S.; Liu, X.; Xiang, H. UV-induced disulfide metathesis: Strengthening interlayer adhesion and rectifying warped 3D printed materials. *Addit. Manuf.* **2022**, *59*, 103085. [CrossRef]
97. Xiang, H.; Yin, J.; Lin, G.; Liu, X.; Rong, M.; Zhang, M. Photo-crosslinkable, self-healable and reprocessable rubbers. *Chem. Eng. J.* **2019**, *358*, 878–890. [CrossRef]
98. Olikagu, C.; Khoshsorour, S.; Dulam, S.D.; Yu, H.-S.; Graham, N.A.; Kim, K.-J.; Jeong, B.; Hedrick, J.L.; Bunnag-Stoner, A.; Cheng, K.; et al. Photopolymer Resins from Sulfenyl Chloride Commodity Chemicals for Plastic Optics, Photopatterning and 3D-Printing. *Adv. Mater.* **2025**, *37*, 2418149. [CrossRef]
99. Li, X.; Yu, R.; He, Y.; Zhang, Y.; Yang, X.; Zhao, X.; Huang, W. Self-Healing Polyurethane Elastomers Based on a Disulfide Bond by Digital Light Processing 3D Printing. *ACS Macro Lett.* **2019**, *8*, 1511–1516. [CrossRef]
100. Feitosa, L.F.; Campos, R.B.; Richter, W.E. Energetics and electronics of polar Diels–Alder reactions at the atomic level: QTAIM and IQA analyses of complete IRC paths. *J. Mol. Graph. Model.* **2023**, *118*, 108326. [CrossRef]
101. Lording, W.J.; Fallon, T.; Sherburn, M.S.; Paddon-Row, M.N. The simplest Diels–Alder reactions are not endo-selective. *Chem. Sci.* **2020**, *11*, 11915–11926. [CrossRef]
102. Roh, S.; Nam, Y.; Nguyen, M.T.N.; Han, J.-H.; Lee, J.S. Dynamic Covalent Bond-Based Polymer Chains Operating Reversibly with Temperature Changes. *Molecules* **2024**, *29*, 3261. [CrossRef]
103. Yang, K.; Grant, J.C.; Lamey, P.; Joshi-Imre, A.; Lund, B.R.; Smaldone, R.A.; Voit, W. Diels–Alder Reversible Thermoset 3D Printing: Isotropic Thermoset Polymers via Fused Filament Fabrication. *Adv. Funct. Mater.* **2017**, *27*, 1700318. [CrossRef]
104. Durand-Silva, A.; Cortés-Guzmán, K.P.; Johnson, R.M.; Perera, S.D.; Diwakara, S.D.; Smaldone, R.A. Balancing Self-Healing and Shape Stability in Dynamic Covalent Photoresins for Stereolithography 3D Printing. *ACS Macro Lett.* **2021**, *10*, 486–491. [CrossRef] [PubMed]
105. Li, X.; Yu, R.; He, Y.; Zhang, Y.; Yang, X.; Zhao, X.; Huang, W. Four-dimensional printing of shape memory polyurethanes with high strength and recyclability based on Diels-Alder chemistry. *Polymer* **2020**, *200*, 122532. [CrossRef]
106. Kaneko, T.; Garcia, R.V.; Chau, A.L.; Pitenis, A.A.; Huang, S.; Moran, B.D.; Bailey, S.J.; Hawker, C.J.; Read de Alaniz, J. Radical-Free Digital Light Processing 3D Printing of Hydrogels Using a Photo-Caged Cyclopentadiene Diels–Alder Strategy. *Adv. Funct. Mater.* **2025**, e14415. [CrossRef]
107. Teotonico, J.; Mantione, D.; Ballester-Bayarri, L.; Ximenis, M.; Sardon, H.; Ballard, N.; Ruipérez, F. A combined computational and experimental study of metathesis and nucleophile-mediated exchange mechanisms in boronic ester-containing vitrimers. *Polym. Chem.* **2024**, *15*, 181–192. [CrossRef]
108. Ono, K.; Tohyama, Y.; Uchikura, T.; Kikuchi, Y.; Fujii, K.; Uekusa, H.; Iwasawa, N. Control of the reversibility during boronic ester formation: Application to the construction of ferrocene dimers and trimers. *Dalton Trans.* **2017**, *46*, 2370–2376. [CrossRef]
109. Lee, J.; Park, J.M.; Jang, W.-D. Fructose-sensitive thermal transition behaviour of boronic ester-bearing telechelic poly(2-isopropyl-2-oxazoline). *Chem. Commun.* **2019**, *55*, 3343–3346. [CrossRef]
110. Wanasinghe, S.V.; Dodo, O.J.; Konkolewicz, D. Dynamic Bonds: Adaptable Timescales for Responsive Materials. *Angew. Chem. Int. Ed.* **2022**, *61*, e202206938. [CrossRef]
111. Bonacini, A.; Saccani, E.; Sciancalepore, C.; Milanese, D.; Drago, G.; Pedrini, A.; Pinalli, R.; Nicolaÿ, R.; Dalcanale, E. Boronate Esters Dynamic Networks for the Reduction of Mechanical Anisotropy in Vat 3D Printed Manufacts. *ACS Appl. Polym. Mater.* **2025**, *7*, 2624–2632. [CrossRef]
112. Sinawehl, L.; Wolff, R.; Koch, T.; Stampfl, J.; Liska, R.; Baudis, S. Photopolymers Based on Boronic Esters for the Enhanced Degradation of 3D-Printed Scaffolds. *ACS Appl. Polym. Mater.* **2023**, *5*, 5758–5771. [CrossRef]
113. Robinson, L.L.; Self, J.L.; Fusi, A.D.; Bates, M.W.; Read de Alaniz, J.; Hawker, C.J.; Bates, C.M.; Sample, C.S. Chemical and Mechanical Tunability of 3D-Printed Dynamic Covalent Networks Based on Boronate Esters. *ACS Macro Lett.* **2021**, *10*, 857–863. [CrossRef]
114. Jia, Y.; Delaittre, G.; Tsotsalas, M. Covalent Adaptable Networks Based on Dynamic Alkoxyamine Bonds. *Macromol. Mater. Eng.* **2022**, *307*, 2200178. [CrossRef]
115. Schulte, B.; Tsotsalas, M.; Becker, M.; Studer, A.; De Cola, L. Dynamic Microcrystal Assembly by Nitroxide Exchange Reactions. *Angew. Chem. Int. Ed.* **2010**, *49*, 6881–6884. [CrossRef] [PubMed]
116. Guillaneuf, Y.; Gigmes, D.; Marque, S.R.A.; Tordo, P.; Bertin, D. Nitroxide-Mediated Polymerization of Methyl Methacrylate Using an SG1-Based Alkoxyamine: How the Penultimate Effect Could Lead to Uncontrolled and Unliving Polymerization. *Macromol. Chem. Phys.* **2006**, *207*, 1278–1288. [CrossRef]
117. Gryn'ova, G.; Lin, C.Y.; Coote, M.L. Which side-reactions compromise nitroxide mediated polymerization? *Polym. Chem.* **2013**, *4*, 3744–3754. [CrossRef]
118. Tran, H.B.D.; Vazquez-Martel, C.; Catt, S.O.; Jia, Y.; Tsotsalas, M.; Spiegel, C.A.; Blasco, E. 4D Printing of Adaptable "Living" Materials Based on Alkoxyamine Chemistry. *Adv. Funct. Mater.* **2024**, *34*, 2315238. [CrossRef]

119. Jia, Y.; Spiegel, C.A.; Diehm, J.; Zimmermann, D.; Huber, B.; Mutlu, H.; Franzreb, M.; Wilhelm, M.; Théato, P.; Blasco, E.; et al. Investigating Dynamic Changes in 3D-Printed Covalent Adaptable Polymer Networks. *Macromol. Mater. Eng.* **2024**, *309*, 2300438. [CrossRef]
120. Wu, X.; Leuschel, B.; Nam, N.H.; Guillaneuf, Y.; Gigmes, D.; Clément, J.-L.; Spangenberg, A. Surface Modification of 3D-Printed Micro- and Macro-Structures via In Situ Nitroxide-Mediated Radical Photopolymerization. *Adv. Funct. Mater.* **2024**, *34*, 2312211. [CrossRef]
121. Belqat, M.; Wu, X.; Morris, J.; Mougin, K.; Petithory, T.; Pieuchot, L.; Guillaneuf, Y.; Gigmes, D.; Clément, J.-L.; Spangenberg, A. Customizable and Reconfigurable Surface Properties of Printed Micro-objects by 3D Direct Laser Writing via Nitroxide Mediated Photopolymerization. *Adv. Funct. Mater.* **2023**, *33*, 2211971. [CrossRef]
122. Wu, X.; Gross, B.; Leuschel, B.; Mougin, K.; Dominici, S.; Gree, S.; Belqat, M.; Tkachenko, V.; Cabannes-Boué, B.; Chemtob, A.; et al. On-Demand Editing of Surface Properties of Microstructures Made by 3D Direct Laser Writing via Photo-Mediated RAFT Polymerization. *Adv. Funct. Mater.* **2022**, *32*, 2109446. [CrossRef]
123. Levenhagen, N.P.; Dadmun, M.D. Bimodal molecular weight samples improve the isotropy of 3D printed polymeric samples. *Polymer* **2017**, *122*, 232–241. [CrossRef]
124. Bischoff, D.J.; Mackay, M.E. Plasticization of a Diels–Alder Covalent Adaptable Network for Fused Filament Fabrication. *ACS Appl. Polym. Mater.* **2024**, *6*, 3335–3341. [CrossRef]
125. Ouyang, H.; Li, X.; Lu, X.; Xia, H. Selective Laser Sintering 4D Printing of Dynamic Cross-linked Polyurethane Containing Diels–Alder Bonds. *ACS Appl. Polym. Mater.* **2022**, *4*, 4035–4046. [CrossRef]
126. Zhou, Q.; Gardea, F.; Sang, Z.; Lee, S.; Pharr, M.; Sukhishvili, S.A. A Tailorable Family of Elastomeric-to-Rigid, 3D Printable, Interbonding Polymer Networks. *Adv. Funct. Mater.* **2020**, *30*, 2002374. [CrossRef]
127. Ying, H.; Zhang, Y.; Cheng, J. Dynamic urea bond for the design of reversible and self-healing polymers. *Nat. Commun.* **2014**, *5*, 3218. [CrossRef] [PubMed]
128. Spitzbarth, B.; Eelkema, R. Properties and applications of dynamic covalent ureas. *Cell Rep. Phys. Sci.* **2024**, *5*, 102010. [CrossRef]
129. Chuo, T.-W.; Hou, J.-T.; Liu, Y.-L. Preparation of polymers possessing dynamic N-hindered amide bonds through ketene-based chemistry for repairable anticorrosion coatings. *Mater. Adv.* **2021**, *2*, 3993–3999. [CrossRef]
130. Wang, J.; Hu, S.; Yang, B.; Jin, G.; Zhou, X.; Lin, X.; Wang, R.; Lu, Y.; Zhang, L. Novel Three-Dimensional-Printing Strategy Based on Dynamic Urea Bonds for Isotropy and Mechanical Robustness of Large-Scale Printed Products. *ACS Appl. Mater. Interfaces* **2022**, *14*, 1994–2005. [CrossRef]
131. Li, X.; Ouyang, H.; Sun, S.; Wang, J.; Fei, G.; Xia, H. Selective Laser Sintering for Electrically Conductive Poly(dimethylsiloxane) Composites with Self-Healing Lattice Structures. *ACS Appl. Polym. Mater.* **2023**, *5*, 2944–2955. [CrossRef]
132. Chen, F.; Gao, F.; Ge, Y.; Guo, X.; Shen, L.; Yang, Y.; Gao, X.; Chen, Y. Tailoring dynamic mechanism of covalent adaptable polyurea networks by varying the category of isocyanates. *Eur. Polym. J.* **2024**, *207*, 112826. [CrossRef]
133. Wang, Z.; Gangarapu, S.; Escorihuela, J.; Fei, G.; Zuilhof, H.; Xia, H. Dynamic covalent urea bonds and their potential for development of self-healing polymer materials. *J. Mater. Chem. A* **2019**, *7*, 15933–15943. [CrossRef]
134. Ying, H.; Cheng, J. Hydrolyzable Polyureas Bearing Hindered Urea Bonds. *JACS* **2014**, *136*, 16974–16977. [CrossRef] [PubMed]
135. Kim, J.G.; Lee, G.S.; Lee, A. Triazabicyclodecene: A versatile catalyst for polymer synthesis. *J. Polym. Sci.* **2024**, *62*, 42–91. [CrossRef]
136. Nifant'ev, I.E.; Shlyakhtin, A.V.; Tavtorkin, A.N.; Kosarev, M.A.; Gavrilov, D.E.; Komarov, P.D.; Ilyin, S.O.; Karchevsky, S.G.; Ivchenko, P.V. Mechanistic study of transesterification in TBD-catalyzed ring-opening polymerization of methyl ethylene phosphate. *Eur. Polym. J.* **2019**, *118*, 393–403. [CrossRef]
137. Soenen, W.; Poilvet, G.; Sekar, A.; Dul, S.; Hervieu, C.; Gaan, S. Reactive extrusion of vitrimers: A short review. *Sustain. Mater. Technol.* **2025**, *45*, e01638. [CrossRef]
138. Altuna, F.I.; Hoppe, C.E.; Williams, R.J.J. Epoxy vitrimers with a covalently bonded tertiary amine as catalyst of the transesterification reaction. *Eur. Polym. J.* **2019**, *113*, 297–304. [CrossRef]
139. Kaur, G.; Kumar, P.; Sonne, C. Synthesis, properties and biomedical perspective on vitrimers—Challenges & opportunities. *RSC Appl. Interfaces* **2024**, *1*, 846–867.
140. Joe, J.; Shin, J.; Choi, Y.-S.; Hwang, J.H.; Kim, S.H.; Han, J.; Park, B.; Lee, W.; Park, S.; Kim, Y.S.; et al. A 4D Printable Shape Memory Vitrimer with Repairability and Recyclability through Network Architecture Tailoring from Commercial Poly(ε-caprolactone). *Adv. Sci.* **2021**, *8*, 2103682. [CrossRef]
141. Prasanna Kar, G.; Lin, X.; Terentjev, E.M. Fused Filament Fabrication of a Dynamically Crosslinked Network Derived from Commodity Thermoplastics. *ACS Appl. Polym. Mater.* **2022**, *4*, 4364–4372. [CrossRef]
142. Choi, S.; Park, B.; Jo, S.; Seo, J.H.; Lee, W.; Kim, D.-G.; Lee, K.B.; Kim, Y.S.; Park, S. Weldable and Reprocessable Shape Memory Epoxy Vitrimer Enabled by Controlled Formulation for Extrusion-Based 4D Printing Applications. *Adv. Eng. Mater.* **2022**, *24*, 2101497. [CrossRef]

143. He, X.; Lin, Y.; Ding, Y.; Abdullah, A.M.; Lei, Z.; Han, Y.; Shi, X.; Zhang, W.; Yu, K. Reshapeable, rehealable and recyclable sensor fabricated by direct ink writing of conductive composites based on covalent adaptable network polymers. *Int. J. Extreme Manuf.* **2022**, *4*, 015301. [CrossRef]
144. Roig, A.; Hidalgo, P.; Ramis, X.; De la Flor, S.; Serra, À. Vitrimeric Epoxy-Amine Polyimine Networks Based on a Renewable Vanillin Derivative. *ACS Appl. Polym. Mater.* **2022**, *4*, 9341–9350. [CrossRef]
145. Grosjean, M.; Guth, L.; Déjean, S.; Paniagua, C.; Nottelet, B. Dynamic and Degradable Imine-Based Networks for 3D-Printing of Soft Elastomeric Self-Healable Devices. *Adv. Mater. Interfaces* **2023**, *10*, 2300066. [CrossRef]
146. Kim, S.; Rahman, M.A.; Arifuzzaman, M.; Gilmer, D.B.; Li, B.; Wilt, J.K.; Lara-Curzio, E.; Saito, T. Closed-loop additive manufacturing of upcycled commodity plastic through dynamic cross-linking. *Sci. Adv.* **2022**, *8*, eabn6006. [CrossRef]
147. Peng, W.; Xia, H.; Wu, J.; Fang, Z.; Zhang, X. Dynamic Boronate Ester Chemistry Facilitating 3D Printing Interlayer Adhesion and Modular 4D Printing of Polylactic Acid. *Adv. Funct. Mater.* **2025**, *35*, 2503682. [CrossRef]
148. Terriac, L.; Helesbeux, J.-J.; Maugars, Y.; Guicheux, J.; Tibbitt, M.W.; Delplace, V. Boronate Ester Hydrogels for Biomedical Applications: Challenges and Opportunities. *Chem. Mater.* **2024**, *36*, 6674–6695. [CrossRef]
149. Amaral, A.J.R.; Gaspar, V.M.; Lavrador, P.; Mano, J.F. Double network laminarin-boronic/alginate dynamic bioink for 3D bioprinting cell-laden constructs. *Biofabrication* **2021**, *13*, 035045. [CrossRef]
150. Kang, B.; Kalow, J.A. Internal and External Catalysis in Boronic Ester Networks. *ACS Macro Lett.* **2022**, *11*, 394–401. [CrossRef] [PubMed]
151. Feng, Q.; Li, D.; Li, Q.; Li, H.; Wang, Z.; Zhu, S.; Lin, Z.; Cao, X.; Dong, H. Assembling Microgels via Dynamic Cross-Linking Reaction Improves Printability, Microporosity, Tissue-Adhesion, and Self-Healing of Microgel Bioink for Extrusion Bioprinting. *ACS Appl. Mater. Interfaces* **2022**, *14*, 15653–15666. [CrossRef] [PubMed]
152. Caliari, S.R.; Burdick, J.A. A practical guide to hydrogels for cell culture. *Nat. Methods* **2016**, *13*, 405–414. [CrossRef] [PubMed]
153. Nguyen, J.K.; Park, D.J.; Skousen, J.L.; Hess-Dunning, A.E.; Tyler, D.J.; Rowan, S.J.; Weder, C.; Capadona, J.R. Mechanically-compliant intracortical implants reduce the neuroinflammatory response. *J. Neural Eng.* **2014**, *11*, 056014. [CrossRef]
154. Childs, A.; Li, H.; Lewittes, D.M.; Dong, B.; Liu, W.; Shu, X.; Sun, C.; Zhang, H.F. Fabricating customized hydrogel contact lens. *Sci. Rep.* **2016**, *6*, 34905. [CrossRef] [PubMed]
155. Peel, A.; Bennion, D.; Horne, R.; Hansen, M.R.; Guymon, C.A. Photografted Zwitterionic Hydrogel Coating Durability for Reduced Foreign Body Response to Cochlear Implants. *ACS Appl. Bio Mater.* **2024**, *7*, 3124–3135. [CrossRef] [PubMed]
156. Hull, S.M.; Lou, J.; Lindsay, C.D.; Navarro, R.S.; Cai, B.; Brunel, L.G.; Westerfield, A.D.; Xia, Y.; Heilshorn, S.C. 3D bioprinting of dynamic hydrogel bioinks enabled by small molecule modulators. *Sci. Adv.* **2023**, *9*, eade7880. [CrossRef] [PubMed]
157. Tavakoli, S.; Krishnan, N.; Mokhtari, H.; Oommen, O.P.; Varghese, O.P. Fine-tuning Dynamic Cross–linking for Enhanced 3D Bioprinting of Hyaluronic Acid Hydrogels. *Adv. Funct. Mater.* **2024**, *34*, 2307040. [CrossRef]
158. Lee, H.-P.; Davis, R.; Wang, T.-C.; Deo, K.A.; Cai, K.X.; Alge, D.L.; Lele, T.P.; Gaharwar, A.K. Dynamically Cross-Linked Granular Hydrogels for 3D Printing and Therapeutic Delivery. *ACS Appl. Bio Mater.* **2023**, *6*, 3683–3695. [CrossRef]
159. Sudhakar, K.; Ji, S.m.; Kummara, M.R.; Han, S.S. Recent Progress on Hyaluronan-Based Products for Wound Healing Applications. *Pharmaceutics* **2022**, *14*, 2235. [CrossRef]
160. Sarker, B.; Papageorgiou, D.G.; Silva, R.; Zehnder, T.; Gul-E-Noor, F.; Bertmer, M.; Kaschta, J.; Chrissafis, K.; Detsch, R.; Boccaccini, A.R. Fabrication of alginate–gelatin crosslinked hydrogel microcapsules and evaluation of the microstructure and physico-chemical properties. *J. Mater. Chem. B* **2014**, *2*, 1470–1482. [CrossRef]
161. Shen, Z.; Zhang, C.; Wang, T.; Xu, J. Advances in Functional Hydrogel Wound Dressings: A Review. *Polymers* **2023**, *15*, 2000. [CrossRef]
162. Zhang, L.; Luo, B.; An, Z.; Zheng, P.; Liu, Y.; Zhao, H.; Zhang, Z.; Gao, T.; Cao, Y.; Zhang, Y.; et al. MMP-Responsive Nanoparticle-Loaded, Injectable, Adhesive, Self-Healing Hydrogel Wound Dressing Based on Dynamic Covalent Bonds. *Biomacromolecules* **2023**, *24*, 5769–5779. [CrossRef]
163. Lin, Z.; Xie, W.; Cui, Z.; Huang, J.; Cao, H.; Li, Y. 3D printed alginate/gelatin-based porous hydrogel scaffolds to improve diabetic wound healing. *Giant* **2023**, *16*, 100185. [CrossRef]
164. Fayyazbakhsh, F.; Khayat, M.J.; Leu, M.C. 3D-Printed Gelatin-Alginate Hydrogel Dressings for Burn Wound Healing: A Comprehensive Study. *IJB* **2022**, *8*, 618. [CrossRef] [PubMed]
165. Joshi, A.; Kaur, T.; Joshi, A.; Gugulothu, S.B.; Choudhury, S.; Singh, N. Light-Mediated 3D Printing of Micro-Pyramid-Decorated Tailorable Wound Dressings with Endogenous Growth Factor Sequestration for Improved Wound Healing. *ACS Appl. Mater. Interfaces* **2023**, *15*, 327–337. [CrossRef] [PubMed]
166. Monavari, M.; Homaeigohar, S.; Medhekar, R.; Nawaz, Q.; Monavari, M.; Zheng, K.; Boccaccini, A.R. A 3D-Printed Wound-Healing Material Composed of Alginate Dialdehyde–Gelatin Incorporating Astaxanthin and Borate Bioactive Glass Microparticles. *ACS Appl. Mater. Interfaces* **2023**, *15*, 50626–50637. [CrossRef] [PubMed]
167. Bonardd, S.; Nandi, M.; Hernández García, J.I.; Maiti, B.; Abramov, A.; Díaz Díaz, D. Self-Healing Polymeric Soft Actuators. *Chem. Rev.* **2023**, *123*, 736–810. [CrossRef]

168. Qiu, X.; Zhang, X. Self-healing polymers for soft actuators and robots. *J. Polym. Sci.* **2024**, *62*, 3137–3155. [CrossRef]
169. Yu, K.; Shi, Q.; Li, H.; Jabour, J.; Yang, H.; Dunn, M.L.; Wang, T.; Qi, H.J. Interfacial welding of dynamic covalent network polymers. *J. Mech. Phys. Solids* **2016**, *94*, 1–17. [CrossRef]
170. Khairkkar, S.; Pansare, A.V.; Pansare, S.V.; Chhatre, S.Y.; Sakamoto, J.; Barbezat, M.; Terrasi, G.P.; Patil, V.R.; Nagarkar, A.A.; Naito, M. Adhesive-less bonding of incompatible thermosetting materials. *RSC Appl. Polym.* **2024**, *3*, 247–256. [CrossRef]
171. Putnam-Neeb, A.A.; Kaiser, J.M.; Hubbard, A.M.; Street, D.P.; Dickerson, M.B.; Nepal, D.; Baldwin, L.A. Self-healing and polymer welding of soft and stiff epoxy thermosets via silanolates. *Adv. Compos. Hybrid Mater.* **2022**, *5*, 3068–3080. [CrossRef]
172. Xu, H.; Liang, H.; Yang, Y.; Liu, Y.; He, E.; Yang, Z.; Wang, Y.; Wei, Y.; Ji, Y. Rejuvenating liquid crystal elastomers for self-growth. *Nat. Commun.* **2024**, *15*, 7381. [CrossRef]
173. Wu, Y.; Zhang, S.; Yang, Y.; Li, Z.; Wei, Y.; Ji, Y. Locally controllable magnetic soft actuators with reprogrammable contraction-derived motions. *Sci. Adv.* **2022**, *8*, eabo6021. [CrossRef] [PubMed]
174. Davidson, E.C.; Kotikian, A.; Li, S.; Aizenberg, J.; Lewis, J.A. 3D Printable and Reconfigurable Liquid Crystal Elastomers with Light-Induced Shape Memory via Dynamic Bond Exchange. *Adv. Mater.* **2020**, *32*, 1905682. [CrossRef] [PubMed]
175. Gomez, E.F.; Wanasinghe, S.V.; Flynn, A.E.; Dodo, O.J.; Sparks, J.L.; Baldwin, L.A.; Tabor, C.E.; Durstock, M.F.; Konkolewicz, D.; Thrasher, C.J. 3D-Printed Self-Healing Elastomers for Modular Soft Robotics. *ACS Appl. Mater. Interfaces* **2021**, *13*, 28870–28877. [CrossRef] [PubMed]
176. Yu, X.; Liu, C.; Wang, L.; Li, T.; Yuan, L.; Yang, J.; Xiao, R.; Wang, Z. 3D printing of reprogrammable liquid crystal elastomers with exchangeable boronic ester bonds. *Giant* **2024**, *20*, 100331. [CrossRef]
177. Zhu, G.; Hou, Y.; Xia, N.; Wang, X.; Zhang, C.; Zheng, J.; Jin, D.; Zhang, L. Fully Recyclable, Healable, Soft, and Stretchable Dynamic Polymers for Magnetic Soft Robots. *Adv. Funct. Mater.* **2023**, *33*, 2300888. [CrossRef]
178. Mannsfeld, S.C.B.; Tee, B.C.K.; Stoltenberg, R.M.; Chen, C.V.H.H.; Barman, S.; Muir, B.V.O.; Sokolov, A.N.; Reese, C.; Bao, Z. Highly sensitive flexible pressure sensors with microstructured rubber dielectric layers. *Nat. Mater.* **2010**, *9*, 859–864. [CrossRef]
179. Jo, Y.; Lee, Y.; Kwon, J.; Kim, S.; Ryu, G.; Yun, S.; Baek, S.; Ko, H.; Jung, S. 3D active-matrix multimodal sensor arrays for independent detection of pressure and temperature. *Sci. Adv.* **2025**, *11*, eads4516. [CrossRef]
180. Chen, J.; Pei, Z.; Chai, B.; Jiang, P.; Ma, L.; Zhu, L.; Huang, X. Engineering the Dielectric Constants of Polymers: From Molecular to Mesoscopic Scales. *Adv. Mater.* **2024**, *36*, 2308670. [CrossRef]
181. Wu, S.; Yang, C.; Hu, J.; Pan, M.; Qiu, W.; Guo, Y.; Sun, K.; Xu, Y.; Li, P.; Peng, J.; et al. Wide-Range Linear Iontronic Pressure Sensor with Two-Scale Random Microstructured Film for Underwater Detection. *ACS Omega* **2022**, *7*, 43923–43933. [CrossRef]
182. Smith-Jones, J.; Ballinger, N.; Sadaba, N.; Lopez de Pariza, X.; Yao, Y.; Craig, S.L.; Sardon, H.; Nelson, A. 3D printed modular piezoionic sensors using dynamic covalent bonds. *RSC Appl. Polym.* **2024**, *2*, 434–443. [CrossRef]
183. Zhang, J.; Wang, Y.; Wei, Q.; Wang, Y.; Li, M.; Li, D.; Zhang, L. A 3D printable, highly stretchable, self-healing hydrogel-based sensor based on polyvinyl alcohol/sodium tetraborate/sodium alginate for human motion monitoring. *J. Biol. Macromol.* **2022**, *219*, 1216–1226. [CrossRef]
184. Zhang, M.; Tao, X.; Yu, R.; He, Y.; Li, X.; Chen, X.; Huang, W. Self-healing, mechanically robust, 3D printable ionogel for highly sensitive and long-term reliable ionotronics. *J. Mater. Chem. A* **2022**, *10*, 12005–12015. [CrossRef]

Disclaimer/Publisher's Note: The statements, opinions and data contained in all publications are solely those of the individual author(s) and contributor(s) and not of MDPI and/or the editor(s). MDPI and/or the editor(s) disclaim responsibility for any injury to people or property resulting from any ideas, methods, instructions or products referred to in the content.